Marine and Petroleum Geology 81 (2017) 334–360

Contents lists available at ScienceDirect

Marine and Petroleum Geology

journal homepage: www.elsevier.com/locate/marpetgeo

Research paper

Structural and facies architecture of a diapir-related carbonate minibasin (lower and middle Jurassic, High Atlas, Morocco)

Antonio Teixell [a, *], Antonio Barnolas [b], Idoia Rosales [b], María-Luisa Arboleya [a]

[a] Departament de Geologia, Universitat Autònoma de Barcelona, 08193 Bellaterra, Spain
[b] Instituto Geológico y Minero de España, 28760 Tres Cantos, Madrid, Spain

ARTICLE INFO

Article history:
Received 9 June 2016
Received in revised form
16 December 2016
Accepted 7 January 2017
Available online 10 January 2017

Keywords:
Salt tectonics
Minibasin
Carbonate facies
Jurassic
High Atlas
Morocco

ABSTRACT

We report the structural geometry and facies architecture of a small diapir-related carbonate-dominated basin from the Jurassic rift of the Moroccan High Atlas. The Azag minibasin is a lozenge-shaped depocenter completely enclosed by tectonic boundaries that we interpret as welds after former salt anticlines or salt walls. The exposed ca. 3000 m-thick infill of the Azag minibasin is asymmetric; layers are tilted to the W defining a rollover geometry. Areally-restricted sedimentary discontinuities and wedges of growth strata near the basin margins indicate sedimentation contemporaneous with diapiric rise of a Triassic ductile layer. Facies evolution through the basin reflects local accommodation by salt withdrawal and regional events in the High Atlas rift. The early basin infill in the Sinemurian and Pliensbachian shows thickness variations indicative of low-amplitude halokinetic movements, with reduced exposed thicknesses compared to surrounding areas. The exposed Toarcian and Aalenian deposits are also reduced in thickness compared to areas outside the basin. Subsidence increased dramatically in the Bajocian-early Bathonian (?), the main phase of downbuilding, when over 2600 m of carbonates and shales accumulated at a rate > 0.5 mm/a in the depocentral area of the minibasin governed by W-directed salt expulsion. The stratigraphic units distinguished often show maximum thicknesses and deeper facies in the depocentral area, and rapidly change to shallower facies at the basin margins. The Bajocian carbonate facies assemblage of the minibasin include: reservoir facies as microbialite-coral reefs in the basin margins (formed during periods of strong diapir inflation and bathymetric relief), basin-expansive oolite bars (formed during episodes of subdued relief), and organic-rich, dark lime mudstones and shales that show source-rock characteristics. The Azag basin is a good analog for the exploration of salt-related carbonate plays in rifts and continental margins where source-rock and reservoir can form in a same minibasin.

1. Introduction

The mobility of rock salt in sedimentary basins containing evaporitic sequences is being recognized in recent years as a prime factor not only determining the basin structure, but also the facies distribution at the local scale and the occurrence of differential subsidence domains across the basin. While many studies describe the structural geometry and kinematics of a diversity of salt tectonics structures (e.g. see Hudec and Jackson, 2007, 2011 for reviews), less studies document in detail the spatial and temporal evolution of sedimentary facies in relation with diapiric phenomena (e.g. Giles and Lawton, 2002; Giles and Rowan, 2012; Ribes et al., 2015). Reported sedimentary basins influenced by salt tectonics include terrestrial systems (Sivas basin, Paradox basin, Flinders range; Ringenbach et al., 2013; Rowan and Vendeville, 2006; Trudgill, 2011), marine mixed clastic-carbonate systems (La Popa basin; Giles and Lawton, 2002) and carbonate systems (Pyrenees, Atlas Mountains; Canérot et al., 2005; Poprawski et al., 2016; Saura et al., 2014, 2016), many of these being essentially studied from a structural point of view. Detailed sedimentological accounts of fluvial and clastic transitional systems in relation to salt tectonics exist in the literature (e.g. Andrie et al., 2012; Kernen et al., 2012; Matthews et al., 2007; Ribes et al., 2015), whereas salt-related carbonate systems are comparatively less documented. The purpose of this paper is to describe the structural geometry and the facies evolution of a small carbonate depocenter (a minibasin) of

* Corresponding author.
E-mail address: antonio.teixell@uab.es (A. Teixell).

http://dx.doi.org/10.1016/j.marpetgeo.2017.01.003
0264-8172/

Jurassic age developed in the east-central High Atlas of Morocco on the basis of excellent surface exposure.

The Atlas Mountains developed as Cenozoic fold-thrust belts by the tectonic inversion of former rift troughs that opened in Triassic-Jurassic times. Diapirs of a late Triassic evaporitic layer (Keuper facies) during the Jurassic basin opening stage were reported in the High Atlas by Bouchouata et al. (1995), Ettaki et al. (2007) and Teixell et al. (2003). Salt tectonics was emphasized in recent papers by Michard et al. (2011), who interpreted antiformal ridges in the central High Atlas as former diapiric salt walls with complex polyphase evolution, and by Saura et al. (2014), who described the structure of minibasins associated with Jurassic diapirism and provided detailed timing estimates on the basis of halokinetic unconformities and growth strata. As is the case of other mountain belts of the western Tethys domain as the Alps or the Pyrenees, salt walls formed during the rifting stage were rejuvenated during the Cenozoic convergence, which often led to the obliteration of the salt structures rendering them easy to overlook.

The Azag n'Oufelloussene basin (hereafter referred to as the Azag basin) of the central High Atlas near Rich (Fig. 1) is a lozenge-shaped depocenter that was formerly interpreted as a Jurassic pull-apart basin bounded by side-stepping strike-slip faults (Brechbühler et al., 1988; Ibouh et al., 2008). By means of a detailed field structural and sedimentological study, we interpret the basin as a diapir-related minibasin enclosed originally by a polygonal array of salt walls and anticlines, and document a unique assemblage of carbonate facies in relation with halokinetic growth and with regional (rift-related) and local (salt-withdrawal) subsidence. The Azag basin is exceptionally exposed and provides a varied assemblage of carbonate facies that makes it a good field analogue for the exploration of early salt-related basins in the continental margin off north Africa (e.g. Tari et al., 2003; Tari and Jabour, 2013), and for carbonate minibasins in the subsurface elsewhere.

2. Geological setting

The Atlas chains of Morocco are intracontinental mountain belts that formed during the Cenozoic by N-S shortening in the northern African plate. They are composed by two branches, the High and Middle Atlas (Fig. 1), developed from the inversion of orthogonal or oblique rift troughs that opened during the Triassic and Jurassic (Choubert and Faure-Muret, 1962; Mattauer et al., 1977; Schaer,

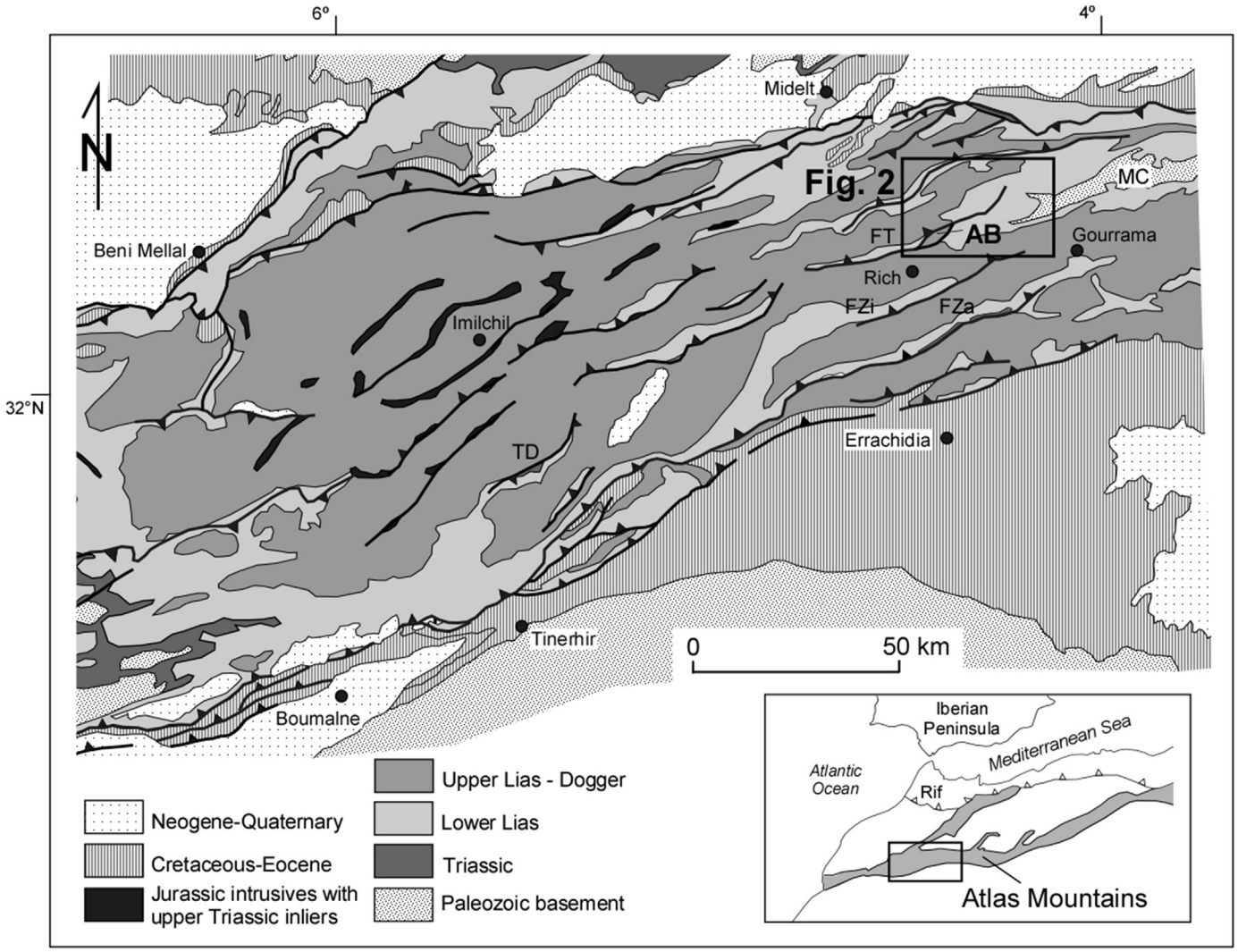

Fig. 1. Geological sketch map of the central High Atlas of Morocco indicating the location of the Azag n'Oufelloussene Jurassic minibasin (AB) (after Teixell et al., 2003). Other localities referred to in the text: FT, Foum Tillicht; FZa, Foum Zabel; Fzi, Foum Zidet; TD, Toumliline salt diapir; MC, Mougueur basement culmination. Jurassic intrusive massifs containing upper Triassic shale, basalt and evaporite inliers have been interpreted as former diapiric ridges (Michard et al., 2011; Saura et al., 2014).

1987; Laville and Piqué, 1992; Beauchamp et al., 1996; Frizon de Lamotte et al., 2000; Teixell et al., 2003; Arboleya et al., 2004). Regional extension direction during the Triassic and Jurassic was oriented NE-SW, with respect to the frame of the present-day African plate (Mattauer et al., 1977; Ait Brahim et al., 2002; El Kochri and Chorowicz, 1996; Piqué et al., 2000; Frizon de Lamotte et al., 2009; Domènech et al., 2015). The location of the ENE-WSW trending central High Atlas coincides with a Jurassic oblique rift that was linked with the Tethys Ocean.

The High Atlas is the most prominent mountain belt of the Atlas system. The central and eastern segments of the High Atlas are dominated by Jurassic sedimentary rocks at the surface, with sparse occurrences of Triassic and Paleozoic rocks (Fig. 1). The tectonic structure of the Jurassic consists of tight anticlines or thrust faults that form calcareous ridges of Liassic limestones and dolomites separated by broad synclines occupied by Upper Lias–Dogger shales (Schaer, 1987; Teixell et al., 2003). Most orogenic shortening in the High Atlas is concentrated in narrow thrust belts in the southern and northern margins (Beauchamp et al., 1999; Benammi et al., 2001; Teixell et al., 2003; Tesón and Teixell, 2008). Variations in Mesozoic stratigraphy and thickness across some thrust faults attest to their origin as synsedimentary extensional faults, which later experienced tectonic inversion. Compressional deformation in the interior of the Atlas is moderate and part of the internal structure was acquired during the Jurassic, as attested by fans of growth strata associated to antiformal and fault ridges. The relict folding during the Jurassic basin-opening stage has been attributed to strike-slip faulting (Laville and Piqué, 1992) or, more recently, to salt diapirism of the Triassic layer (Michard et al., 2011; Saura et al., 2014), an interpretation which we favor.

Basement exposed in the central High Atlas consists of Paleozoic slates affected by the Variscan orogeny, which crop out in thrust-related antiformal culminations as the Mougueur massif located 20 km to the east of the study area (Figs. 1 and 2). Mesozoic sedimentation in the Atlas rift was initiated within small Triassic rift basins that were filled with detrital red beds, basalts and occasional salt occurrences. Lower Lias platform limestones and dolomites sealed the Triassic rifts (Laville et al., 2004). Accommodation by renewed rifting increased in the mid Liassic, and the carbonate platforms were drowned and disrupted by the formation of subsiding basins, where thick successions of limestones, calciturbidites and marls accumulated up to Dogger times (Warme, 1988, and references therein). The Jurassic record ends with Bathonian to Kimmeridgian red beds with numerous discontinuities indicative of a generalized regression (Jenny et al., 1981; Haddoumi et al., 2010). The Atlas rift evolution was accompanied by extensional salt tectonics (Saura et al., 2014) and by the intrusion of mid to late Jurassic alkaline igneous rocks (Hailwood and Mitchell, 1971; Laville and Piqué, 1992). Cretaceous sedimentary rocks, only locally preserved from erosion in the interior of the Atlas belts, overlap the Variscan basement in the present-day forelands of the Atlas Mountains, forming tabular, post-rift deposits (Beauchamp et al., 1996; Teixell et al., 2003).

The Azag minibasin is located in the High Atlas of Rich (Fig. 1). This region shows the characteristic pattern of the interior of the central High Atlas with an anastomosing system of antiformal and faulted ridges of varying E-W to NE-SW trend, with wider synclines in between (Fig. 2). Folds show often sigmoid map patterns;

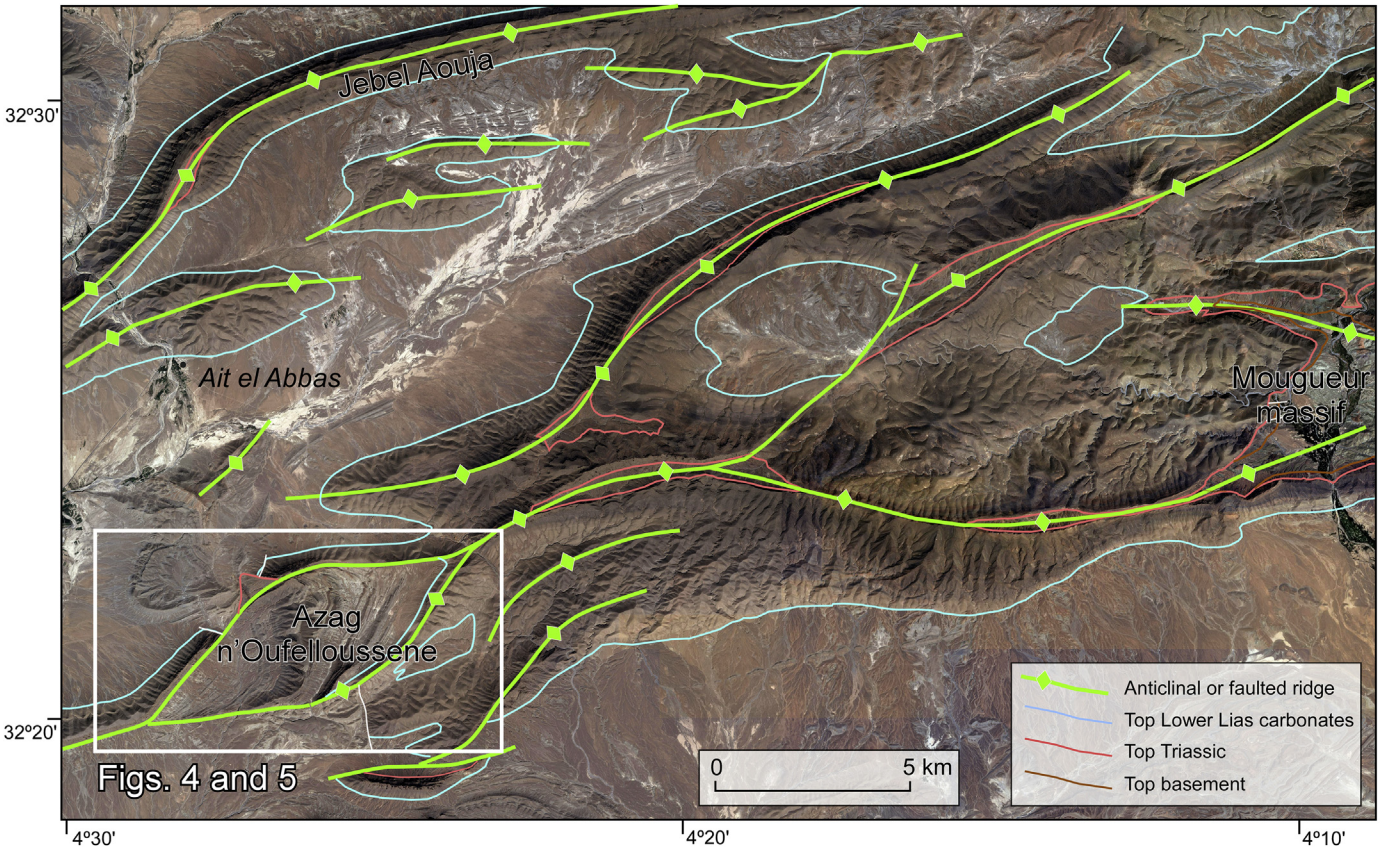

Fig. 2. Google Earth satellite image of part of the High Atlas near Rich (location in Fig. 1), showing a system of anastomosing ridges (in green) and synformal minibasins in between. The studied Azag minibasin is in the lower left. Tight fold ridges are detached in the Triassic, but note that a slate-dominated basement is also locally involved in the folding (Mougueur massif, center right). (For interpretation of the references to colour in this figure legend, the reader is referred to the web version of this article.)

synclinal basins in upper Lias to Dogger shales and carbonates may have oval or polygonal (lozenge-shaped) planforms, as the Azag basin (Fig. 2). Thickness variations and growth strata indicate that folding already started in the Jurassic (e.g. Laville, 1985), although folds and newly formed thrust faults were active during the Cenozoic compression. Tight to isoclinal anticlines defined by lower Lias carbonates suggest detachment in the Triassic level. However, the underlying Paleozoic is also involved in the folding, as observed in the basement exposure at Mougueur (El Kochri and Chorowicz, 1988; Teixell et al., 2003). Triassic shale and basalt in antiformal cores is often concordant with the overlying Liassic overburden, but truncation relationships suggestive of diapiric piercing of the Triassic unit are also observed. Triassic evaporitic rocks are seldom observed at the surface, as also happens in other documented diapiric structures west of the study area (Saura et al., 2014). Equidimensional diapirs or stocks as in other salt fold belts are rare.

The stratigraphic frame of the Jurassic of the High Atlas of Rich has been extensively documented (Du Dresnay, 1971; Studer, 1987; Warme, 1988; Igmoullan et al., 2001; Neuweiler et al., 2001; Wilmsen and Neuweiler, 2008; Ait Addi and Chafiki, 2013 and references herein). As outlined above, the High Atlas Jurassic basin was a Tethyan rift basin, with shallow carbonate platforms surrounding a central trough where deep-water carbonate and marly sedimentation dominated (Evans et al., 1974; Warme, 1988). During the early Jurassic shallow water carbonate sedimentation was general in the basin. Three main phases of platform break-up and collapse are registered, causing platform backstepping and widening progressively the basin trough. The first phase of platform break-up occurred in the early Lotharingian (late Sinemurian) with the drowning of the lower Sinemurian shallow carbonate platform in this area, as documented in the Foum Tillicht (Neuweiler et al., 2001) and Foum Zidet (Wilmsen et al., 2002) sections to the west of the study area (Fig. 1). Far to the east of the Rich area (Djebel Bou Dahar block), this event is recorded in shallow platform deposits by an unconformity marking a change from a ramp geometry to an aggrading to retrograding, steep-flanked carbonate platform (Verwer et al., 2009; Merino-Tomé et al., 2012). In the early Carixian (early Pliensbachian), a new platform break-up was registered by the platform drowning and margin collapse in the Foum Zabel section, to the south of the study area (Neuweiler et al., 2001). The last phase of platform break-up is recorded in the late Pliensbachian by the drowning of the shallow marine platform across the southernmost sections of the High Atlas (Wilmsen and Neuweiler, 2008).

The stratigraphy of the Lower Jurassic (Sinemurian to Pliensbachian) platform margins is described in Wilmsen and Neuweiler (2008) and Lachkar et al. (2009) for the Saharian margin (south) and in Igmoullan et al. (2001) for the Hauts Plateaux margin (north). In the intervening area of Rich (Fig. 1), three superposed sedimentary units have been defined. A basal shallow water carbonate platform unit (Idikel Formation, Hettangian?-early Sinemurian), an intermediate unit of deep-water sponge reefs (Foum Zidet Formation, late Sinemurian), not present everywhere, and an upper distal platform to slope carbonate rhythmite (Ouchbis Formation, Pliensbachian) (Wilmsen and Neuweiler, 2008) (Fig. 3). For the overlying basinal, marly-dominated units (Toarcian to Bathonian), the stratigraphy reported is less consistent. In the central basin trough, which includes the Rich area, French geologists working in early regional mapping projects established the first initial stratigraphic subdivision. Their results are summarized in the schema by Du Dresnay (1971) (Table 1). Studer (1987), who studied the northern margin of the Atlas basin SW of Midelt, defined some of the main lithostratigraphic units that were later widely followed (Table 1). Finally, Ait Addi (1994), Ait Addi et al. (1998) and Ait Addi and Chafiki (2013) gave some further

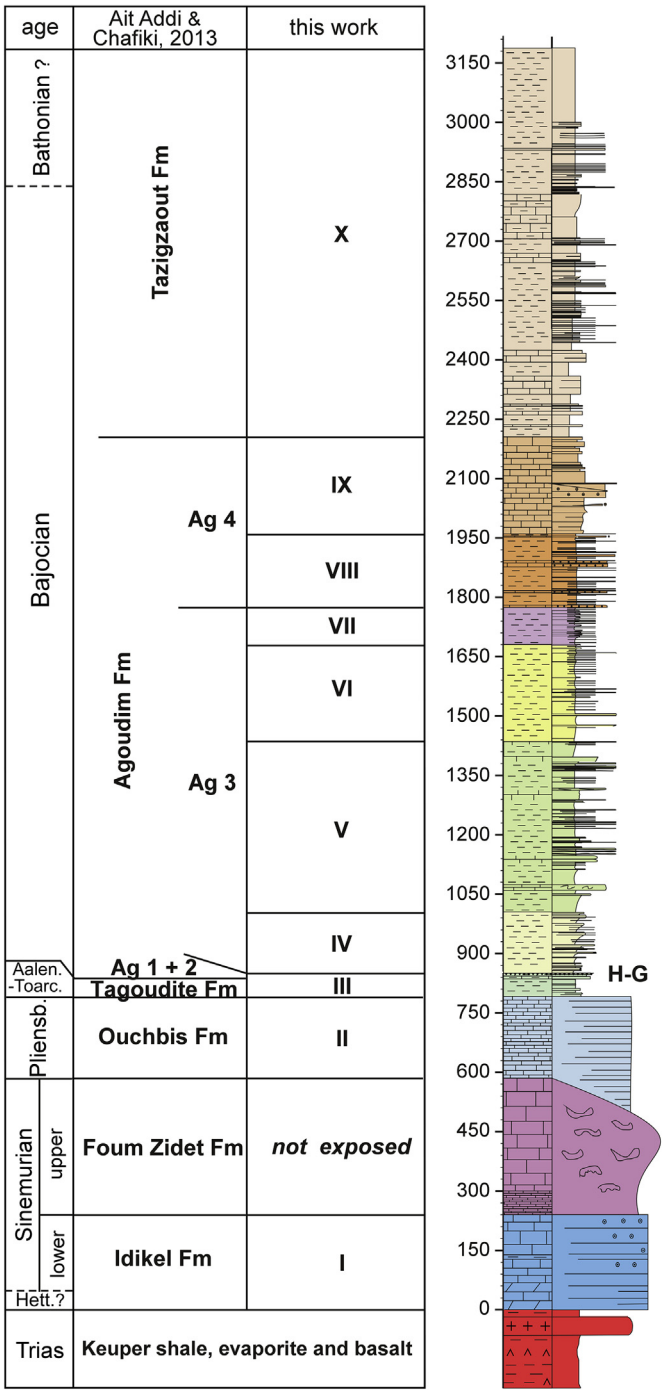

Fig. 3. Synthetic stratigraphic section of the Jurassic of the central High Atlas in the Rich area. Roman numbers indicate the ten units mapped in Fig. 5. H-G: hardground.

contributions to the lithostratigraphic frame as summarized in Table 1 and Fig. 3.

3. Methods

In this study we investigate the structure, the facies evolution and the sedimentation-tectonics relationships of the ca. 3000 m thick infill of the Azag minibasin. The study of the basin is based on detailed geological mapping and field analysis of stratigraphic relationships and lithofacies in the Toarcian to Bajocian-Bathonian? succession. For the latter, composite stratigraphic sections were

Table 1
Equivalence of lithostratigraphic units defined in the Toarcian to Bathonian? deposits of the High Atlas in the Rich area (after du Dresnay, 1971; Stanley, 1981; Studer, 1987; Milhi et al., 2002; Ait Addi, 2000; Ait Addi and Chafiki, 2013).

	du Dresnay, 1971	Stanley, 1981	Studer, 1987	Milhi et al., 2002	Ait Addi, 2000	Ait Addi & Chafiki, 2013
BATHONIAN			ANEMZI Fm	ANEMZI Fm	ANEMZI Fm	ANEMZI Fm
	Marno-calcaires a Pholadomyes		AGOUDIM Fm	TAZEGZAOUT Fm	TAZIGZAOUT Fm	TILLOUGUDITE Fm
BAJOCIAN Upper						TAZIGZAOUT Fm
	Calcaire corniche	E		AGOUDIM Fm	AGOUDIM Fm: Mb IV	AGOUDIM Fm: Ag IV
BAJOCIAN Lower	Marnes a Posidonies	D				
		C			AGOUDIM Fm: Mb III	AGOUDIM Fm: Ag III
AALENIAN		B				
	Calcaires a Cancellophycus	A			AGOUDIM Fm: Mb II	AGOUDIM Fm: Ag II
TOARCIAN Upper					AGOUDIM Fm: Mb I	AGOUDIM Fm: Ag I
TOARCIAN Middle						
TOARCIAN Lower			TAGOUDITE Fm	TAGOUDITE Fm	TAGOUDITE Fm	TAGOUDITE Fm

measured in detail crossing the two margins and the depocenter of the basin, with maximum thickness of ca. 2600 m of measured section in the log of the depocentral area. This sedimentary thickness rapidly decreases towards the northern and southern basin margins, where some of the main stratigraphic units pinch out or change laterally to shallower lithofacies. The geobodies were

Fig. 4. Google Earth satellite image of the Azag minibasin. The area coincides with the geological map of Fig. 5. UTM coordinates, zone 30.

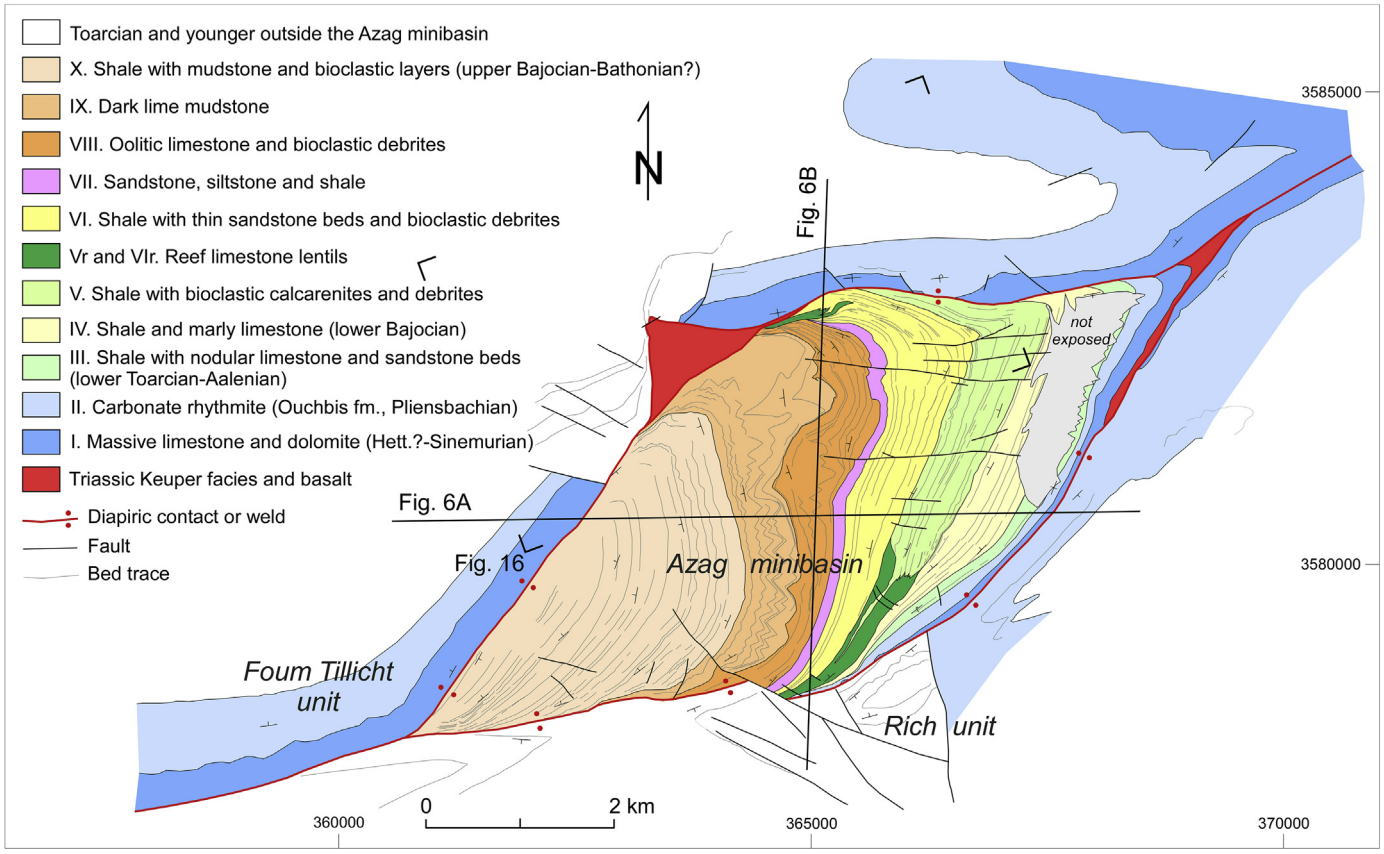

Fig. 5. Geological map of the Azag minibasin (location in Fig.. 1 and 2) showing the stratigraphic units distinguished with internal bed traces, the cross-sections of Fig. 6, and the location of Fig. 16 (box corners). The Triassic stock to the north of the basin contains small bodies of Jurassic gabbro. UTM coordinates, zone 30.

mapped and traced laterally in the field over high-resolution Google satellite images. The aim was to document the lateral variability of the sedimentary thicknesses and lithofacies. In addition, key stratigraphic surfaces and unconformities were recognized and traced across the study area as correlation tie-points between sections. The facies of the two lower stratigraphic units mapped (Hettangian?-Sinemurian to Pliensbachian, Fig. 3), which show rather homogeneous characteristics in and out of the Azag basin, were not studied in detail and the reader is referred to the sedimentological works of Mehdi et al. (2003) and Wilmsen and Neuweiler (2008).

More than 160 thin-sections were prepared from hand rock samples collected during the field surveys, in order to characterize microfacies types and the nature of the carbonate and detrital components of the different lithofacies recognized in the field. Microfacies were analyzed in the laboratory with a *Nikon Eclipse LV 100Pol* petrographic microscope with transmitted and reflected light. When available, ammonites and brachiopods were collected to improve the biostratigraphic frame of the studied sections. The geological map and structural cross-sections were constructed using the *Move* platform of the Midland Valley software. Cross-sections were kinematically restored to selected steps using the built-in *inclined shear* and *flexural-slip unfolding* algorithms.

4. Structure of the Azag minibasin

The Atlas rift experienced moderate inversion and shortening strain during the Cenozoic orogeny. Part of the high topographic elevation of the Atlas system is due to recent long-wavelength uplift (Teixell et al., 2005; Babault et al., 2008), by which the internal attributes of the Jurassic basin are generally well preserved and can be readily investigated (e.g. Saura et al., 2014). Many of the structural features of the Azag basin here described were already acquired during the early and mid Jurassic, with some tightening during the later compressional episode.

The Azag minibasin has a lozenge (rhomboidal) plan shape, ca. 9 km long and 4 km wide, completely enclosed by tectonic boundaries (Figs. 4 and 5). The basin fill is asymmetric, strongly tilted to the W or WNW. A N- to NNE-dipping pressure-solution cleavage, highly transecting the bedding strike, is observed. The boundaries of the basin appear as faulted anticlines; layers usually dip away from the boundaries, i.e. to the interior of the Azag basin or to the adjacent Foum Tillicht and Rich units (Fig. 6). In the eastern boundary of the basin, lower Lias carbonates are at similar elevation in both sides, and exposed at the surface (Fig. 6). In contrast, in the western and northern margins, the Hettangian?-lower Sinemurian Idikel limestones and dolomites of the Foum Tillicht unit are much elevated so the boundary appears at the surface as a steep thrust fault, subparallel to bedding in the western side, but truncating the tilted Lias to Dogger succession of the Azag minibasin in the other side. Remnants of Triassic basalt and red shale are often observed in between the Jurassic beds of the Azag basin and the adjoining units, marking the boundaries. Jurassic rocks immediately adjacent to the boundaries appear sheared, and are occasionally recrystallized and intruded by abundant veins evidencing the circulation of fluids along the margins. No evidence of strike-slip along the basin fault boundaries has been detected.

We interpret the boundaries of the Azag minibasin as salt welds (commonly thrust welds) deriving from the squeezing of former salt anticlines or salt walls. This differs from previous

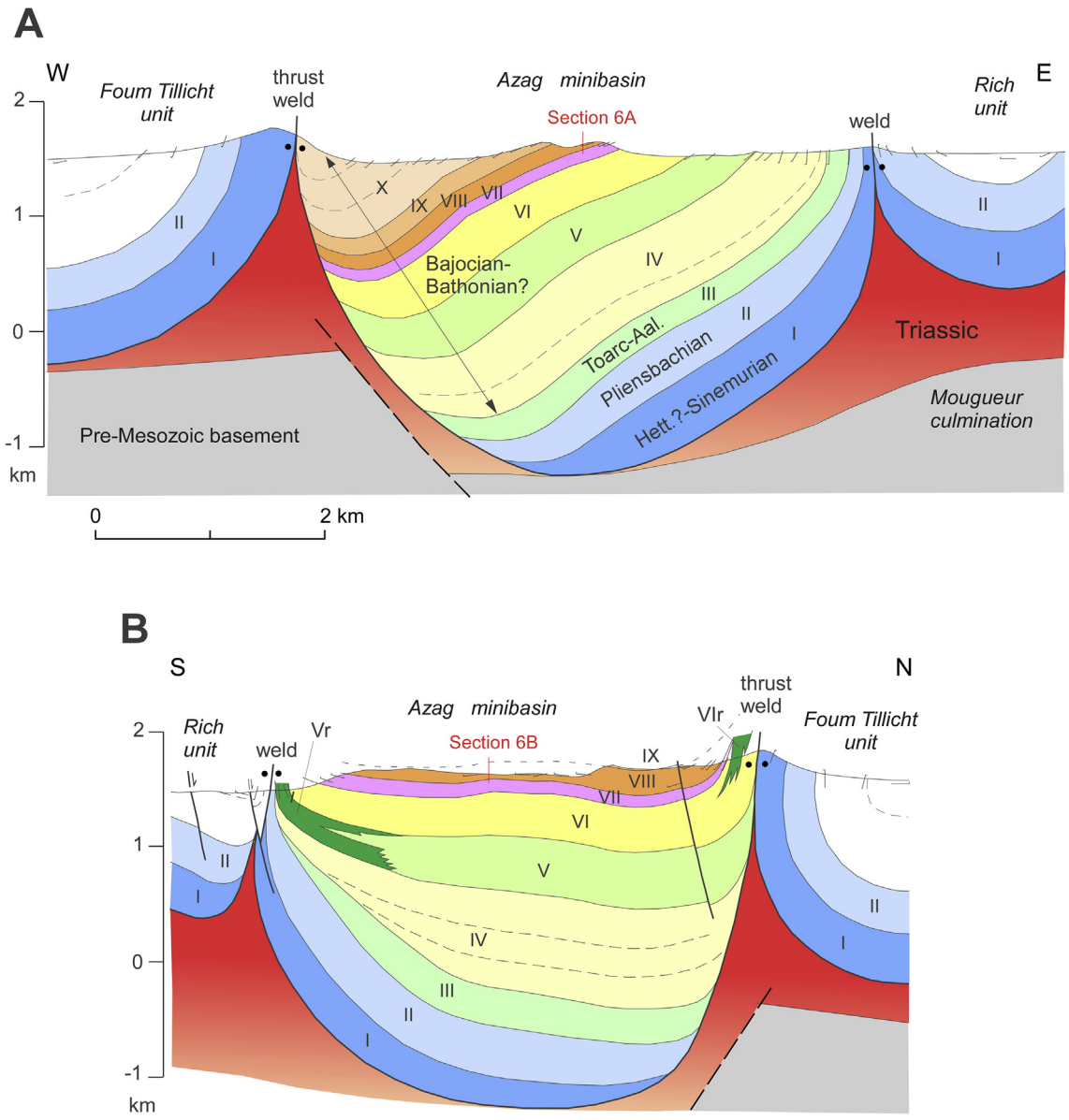

Fig. 6. Geologic cross-sections across the Azag minibasin (no vertical exaggeration, location in Fig. 5). Stratigraphic units as in Figs. 3 and 5.

interpretations by Brechbühler et al. (1988) and Ibouh et al. (2008) that explained the Azag structure as a strike-slip related pull-apart basin in the light of its plan view form. As previously mentioned, evaporitic rocks are not observed at the surface, but salt efflorescences are observed in veins at the southern margin of the Azag minibasin. Triassic halite has been reported in other areas of the central High Atlas (e.g. at Toumliline, Teixell et al., 2003; Fig. 1), and was required in gravity modeling (Ayarza et al., 2005). Consequently, we interpret the Azag depocenter as a salt-withdrawal minibasin formed in between a polygonal system of salt ridges, analogous to the natural and experimental examples described by Rowan and Vendeville (2006), and to the diapiric structures described in the west-central High Atlas by Saura et al. (2014).

An E-W profile of the Azag minibasin shows a marked asymmetric geometry (Fig. 6a). The lower part of the overburden starting from the Idikel Formation dips vertically and has been upturned to surface exposure at 1500 m asl, some 2500 m above the inferred base of the overburden in the minibasin axis. Stratal dip decreases up section, to values of 30–40° W near the western margin of the minibasin, before beds are folded into a narrow syncline paralleling the boundary weld. The deep structure of the western basin margin is not exposed, and has been interpreted as an east-dipping diapir flank analogous to comparable asymmetric minibasins imaged in seismic profiles (e.g. Figs. 14 and 17 in Gómez-Cabrera and Jackson, 2008, Fig. 23 in Hudec et al., 2009). Thickness variations in the deeper parts of the basin indicative of migration of depocenters are not observed in the profile due to the outcrop pattern; on the lack of information, the E-W section was constructed conservatively assuming homogeneous to gently varying thickness deduced from the exposed thickness changes at the surface (Fig. 6a).

A N-S (strike) profile shows a more symmetric bowl shape (Fig. 6b), with upturned layers in both margins, where they are locally arranged in spectacularly exposed fans of progressive unconformities (see below). The maximum stratigraphic thickness is

observed in the minibasin center, and units thin rapidly to the basin margins. Due to layer attitude and to exposure conditions, thickness variations of the individual units are observed in this N-S direction, where the geological map provides a basin-wide profile (Fig. 5). Although local stratigraphic discontinuities exist (see below), hook-type unconformity bounded halokinetic sequences are not observed, with the exception to the proximity of a diapiric stock in the northern margin of the Azag minibasin in the Foum Tillicht unit (Fig. 5 and see below). Units rather conform to wedge type sequences (Giles and Rowan, 2012). The preserved stratigraphic thickness in the Azag minibasin is larger than in the adjacent Rich and Foum Tillicht units (Fig. 6).

5. Lithofacies types

Thirteen depositional lithofacies (F1 to F13) have been differentiated in outcrop according to the lithology, sedimentary structures, bedding, stratal geometries, skeletal and non-skeletal components, fossil content and fossil traces. Lithofacies descriptions have been completed with microfacies observations. The main characteristics of the lithofacies types, organized from shallower to deeper water, are summarized in Table 2.

5.1. Lithofacies F1: coral-microbial boundstone

5.1.1. Description

This lithofacies conforms massive lithosomes, tabular and mound-shaped, a few meters to hundred meters long and up to 20 m thick. They are composed dominantly of corals and micrite and appear in two contexts: a) at the minibasin margin paleohighs, and b) in high-energy settings, within and on top of migrating oolite-skeletal sand bars. The microfacies consists of wackestone to boundstone made of microbialitic crusts with poorly structured thrombolite fabrics (Fig. 7A), and with variable amounts of *in situ* platy and branching corals (Fig. 7B), encrusting micro-organisms and calcimicrobes, encrusting coralline sponges, graded microbial peloids, *Rivulariacean*-type cyanobacteria (Fig. 7C), cryptobiontic *Bullopora*-type calcareous foraminifera and colonies of tube-worms (Fig. 7D). Other components are desmosponge spicules and debris of bivalves, corals, echinoids, gastropods, micritized grains, peloids and scarce benthic foraminifera (valvulinids) embedded in micrite matrix. Corals are often bored by endolithid bivalves and micro-organisms. *Rivulariacean*-type filamentous cyanobacteria may appear as both encrusting forms on the surface of the corals and as cryptobiontic forms inside coral cavities (Fig. 7C). Microbial stromatolitic-thrombolitic structures usually develop around bioclasts and corals. Authigenic quartz crystal with idiomorphic ends and evaporite pseudomorphs (gypsum, celestine) are frequent in the micritic reefal facies at the minibasin margins (Fig. 7E).

5.1.2. Interpretation

The lithology and the biotic association (corals, cyanobacteria) suggest relatively shallow water depths within the photic zone. The presence of micro-encrusters and thrombolites suggests relatively low sedimentation rates for the formation of this lithofacies, because microbial communities are not able to survive high sedimentary inputs (e.g. Dromart, 1992; Olivier et al., 2003; Pleş et al., 2013). Although modern stromatolites and thrombolites may be found in both intertidal and subtidal settings (Riding, 2000), in the fossil record thrombolites more typically occur in subtidal open sea environments with relatively low hydrodynamic conditions (e.g. Dongjie et al., 2013). In the Jurassic, thrombolites become an important constituent of open sea reefs, as seen in other Lias and Dogger reefs and mounds of the High Atlas (Della Porta et al., 2013; Olivier et al., 2013; Tomás et al., 2013) and other Tethyan areas (e.g. Olivier et al., 2003). Therefore, this lithofacies is interpreted as bioconstructions of coral-thrombolite reefs and buildups (patch reefs) developed on top of the diapiric highs, or on prograding grainstone bars when the bars became inactive.

The presence of early diagenetic quartz and evaporite crystals in limestone has been related to depositional hypersaline conditions like those of the sabkha environments (e.g. Friedman and Shulka, 1980). However, other process of production of early diagenetic quartz in limestones under hypersaline conditions and not precisely related to sabkha environment is the formation under saline solutions derived from salt diapirs underlying reefs (Reitner, 1988; Flügel, 2004). A similar relationship between quartz precipitation and hypersaline conditions in diapir-related reefs have been described previously in other limestones growing on salt-diapirs such as the Albian Caniego limestones of northern Spain (Reitner, 1988).

5.2. Lithofacies F2: oolitic grainstones

5.2.1. Description

This lithofacies shows grainstone to packstone texture composed mainly of simple and compound oolites. It is organized in tabular to lensoid and channel-like beds that usually display large-scale trough, high-angle planar and sigmoidal cross-bedding. Thickness of individual beds ranges from about 2 to 30 m. The individual beds are a hundred meters to a few kilometers long, grading laterally and being interbedded with marls. The bases are erosional, especially in channel-like beds, or gradational with rapid coarsening upwards trends. These oolitic beds may display high-angle, large-scale foresets up to 30 m tall, made of avalanche layers with particle-size segregation and normal gradation. Bottomsets are made of horizontal, nodular, bioturbated oolite-skeletal calcarenites and bioclastic marls with brachiopods and thin-bedded turbidites. Topsets are usually absent and represented by a sharp or bioturbated surface covered by bioclastic lags or colonized by mixed oysters-brachiopod communities or by corals.

The oolites are fine-to medium-grained, well-rounded to elongated and moderately to well-sorted (Fig. 8A). Nuclei include limestone intraclasts, bioclasts and idiomorphic quartz (Fig. 8B). Minor components are intraclasts, bioclasts and detrital idiomorphic quartz and evaporite crystals.

5.2.2. Interpretation

These oolitic limestones represent deposition from active shoal complexes. The large-scale cross bedding is suggestive of rapid migration of large bedforms and subaqueous sand-waves and dunes. Oolites most probably formed on the shallow top and where transported downdip from the shoal top, causing the dune migration. The frequent absence of topsets suggests abrasion, probably due to wave action, and non-deposition due to by-pass of sediment. The channel-like beds with erosive bases may represent the infill of channels and slope gullies that transported sediment downdip from the shallow water oolite factory.

5.3. Lithofacies F3: skeletal-intraclastic grainstones

5.3.1. Description

This lithofacies consists of skeletal-intraclastic or mixed skeletal-intraclast- oolite packstone to grainstone, locally rudstone, organized in tabular to lenticular cross-bedded bars and channel-like sand bodies ranging from 1 to 8 m thick and hundred meters of lateral extension. The channelized sand bodies present erosive bases and trough cross-bedding. The grainstone bars display trough cross-bedding and large-scale planar to sigmoidal cross-bedding with avalanche foresets. Laterally, the grainstone beds are of

Table 2
Main lithofacies types of the Toarcian to Bajocian-Bathonian? succession of the Azag minibasin infill.

Code	Lithofacies	Lithology/texture	Sedimentary and biogenic structures and bedding	Microfacies and components	Interpretation	Depositional environment/ Facies associations
F1	Coral-microbial boundstone.	Wackestone to boundstone.	Massive, tabular and mound-shape lenses growing on topographic highs. Few meters to hundred meters long and up to 20 m thick.	Frames of dense micrite matrix with branching and platy corals, *Rivulariacean*-type cyanobacteria, microbial thrombolite crusts, constructive micrite cortices, microbial peloids, worm-tubes colonies, encrusting micro-organism and coralline sponges. Early diagenetic, idiomorphic authigenic quartz crystal and evaporite pseudomorphs.	Microbial-dominated coral reefs forming buildups and isolated miniplatforms on topographic highs. Shallow water within euphotic zone.	Shallow reefal platform
F2	Oolitic grainstone	Oolite grainstone to packstone	Tabular to lensoidal and channel-like beds, 2 to 30 m thick and hundred meters to few kilometers long. Erosional to gradational bases. Trough, planar and sigmoidal, medium to large-scale, cross bedding. High-angle avalanche foresets. Topsets usually absent and represented by sharp to bioturbated surfaces with coral/ oyster colonization.	Fine- to medium-grained oolites, well rounded to elongated. Single or composite. Minor components are oolitic intraclasts, bioclasts, idiomorphic quartz and evaporite pseudomorphs.	Active shoals complexes with subaqueous migration of sand-waves and dunes, and infilling of slope channels-gullies.	Middle ramp shoal complexes
F3	Skeletal-intraclastic grainstone	Skeletal and mixed skeletal-oolitic-intraclast packstone to grainstone.	Tabular to lenticular beds 1-8 m thick, hundred meters long. Trough, planar and sigmoidal, medium to large-scale, cross-bedding with avalanche foresets.	Millimetric to centimetric debris of corals, cyanobacteria, gastropods, echinoderms, bivalves, *Cayeuxia*, *Cladocoropsis*, dasycladalean algae, oolites, limestone intraclasts, sandstone lithoclasts.	Open-sea, high hydrodynamic conditions. Basinward prograding bars and infilling of slope channel-gullies.	
F4	Brachiopod and oyster beds	Brachiopod or mixed brachiopod-oyster rudstones in bioclastic marly matrix.	Massive beds, developed as discrete lumachelic beds 0.15 to 7.5 m thick. Occasionally bioturbated. Sharp bases and tops.	Brachiopod-dominated whole shell concentrations, occasionally along with bivalves and small oyster shells.	These beds appear in two contexts: as in situ colonizations on top or down-dip of the oolitic grainstone bars, and as gravity-driven and reworked material by storms or due to slope instability.	Outer ramp
F5	Sponge wackestone	Dark wackestone to mudstone.	Tabulate to nodular beds up 15 cm thick each, forming packages up to 2 m thick.	Dense micrite matrix with hexactinellid and lithistid siliceous sponge communities, demosponge spicules, peloidal micrite and bioclats. The spicules are unsorted and most likely derived from *in situ* sponge decaying.	Stable and non-turbulent environments in the reefal upper slope, donwdip of the environment of the platy corals. Below the photic zone.	Reefal slope
F6	Lithoclastic-bioclastic rudstone, carbonate breccias and pebbly marls	Clast- to mud-supported breccias and disperse rubbles and limestone clasts in a marly matrix.	Unorganized beds with coral rubbles and limestone clasts up to 30 cm long. Planar to lenticular beds, 0.25 to 7 m thick, structureless to rude laminated. May appear associated to slumped beds.	Coral and limestone clasts. Other components include debris of bivalves, oysters, belemnites, inoceramids, crinoids, etc.	Grain flow, debris flow and rock fall deposits. Reefal platform slope and talus environments.	
F7	Bioclastic marls and marly calcarenites	Massive, muds-upported bioclastic marls and fine-grained muddy calcarenites.	Beds are 0.10–2 m thick, structureless to rude laminated. Bases sharp to slightly erosives. Bioturbated.	Intraclasts, muddy pebbles, brachiopods, remains of crinoids, bivalves, oysters, corals, serpulids.	Muddy debrites associated to gravitational flows: mud-flows to debris flows.	
F8	Interbedded sandstones, siltstones and shales.	Heterolithic, thin-bedded siltstones to fine-grained quartz sandstone interbedded in claystones; and cross-laminated, fine- grained quartz sandstones-siltstones.	Rhythmic bedded shales and sandstones with laterally persistent sandstone thin beds, interbedded in claystones. Individual thin-bedded sandstone beds are up to 15 cm thick, with sharp to erosive bases with sole marks, normal gradation and rippled tops. Cross-laminated fine-grained sandstone beds are up to 0.5 m thick and stack in packages up to 5 m thick. These lithologies are organized in thickening- and coarsening- upward sequences 10 to 60 m thick.	Fine-grained quartz greywackes with coal detritus.	Progradation of delta lobes showing a transition from claystone with turbidites of the prodelta environment to sandier facies of the distal delta front or distal deltaic bars.	Prodelta

Table 2 (*continued*)

Code	Lithofacies	Lithology/texture	Sedimentary and biogenic structures and bedding	Microfacies and components	Interpretation	Depositional environment/ Facies associations
F9	Marls and marly limestones	Greyish marls and marly limestones	Monotonous successions up to 120 m thick. Fissile lamination or nodular bedding.	Scarce belemnites and bioclasts: bivalves, brachiopods, echinoderms, oysters	Outer platform/basin.	Outer platform/ basin
F10	Marls with thin-bedded siltstones and calcisiltites	Heterolithic marls and marly limestones with interbedded thin-bedded siltstone and calcisiltite beds.	Siltstone and calcisiltite beds are 0.5-5 cm thick, with sharp bases and grain gradation and occasionally wavy to ripple lamination at the top.	Scarce bioclast.	Outer platform/basinal deposits with distal tempestites/ turbidites triggered by storms or slope instability.	
F11	Black lime mudstones	Black to dark grey mudstone to wackestone.	Thickening-upward packages, up to 54 m thick, of tabular-bedded limestones. Individual beds are 20 to 50 cm thick. *Chondrites*.	Debris of echinoderms, thin-shelled bivalves, sponge spicules. Frequent framboidal pyrite and pyrite nodules and cubes.	Silled basin with restricted water circulation and poorly-oxygenated sea floor.	
F12	Spiculitic silty marls and limestones	Spiculitic wackestone to packstone, silty spiculitic wackestone and silty-marly limestones.	Massive beds up to 0.60 m thick. Irregular bed tops with nodulization. Stacked in packages up to 6 m thick.	Micrite matrix with well-sorted and angular silt-sized quartz grains, peloids, bioclastic debris, ostracods, rare small benthic foraminifera and frequent monoaxon and triaxon sponge spicules.	Outer platform with some siliciclastic influence.	
F13	Rhythmic bedded and nodular marls and limestones	Marls rhythmically interbedded with marly limestones and bioclastic wackestones.	Grey to yellow marls 0.20 to 2 m thick alternating rhythmically with marly limestones and bioclastic limestones 0.10 to 0.30 m thick. Tabular to nodular bedding. *Cancellophycus*.	Beleminites, ammonites, occasionally plant fragments.	Hemipelagic ramp/outer platform.	
F14	Ferruginous crust	Iron-rich crust	Irregular, 2 to 10 cm thick.	Ferruginous microstromatolite layers with encrusting foraminifera and serpulids. Belemnites, ammonites.	Discontinuity with hardground development. Condensed surface.	

varying thicknesses and change laterally to nodular-bioturbated calcarenites and finally to marls. The microfacies is dominated by fragments of corals, gastropods, echinoderms, brachiopods, bivalves, *Cayeuxia*, *Cladocoropsis*, cyanobacteria, dasycladalean algae, undifferentiated bioclasts, peloids, benthic foraminifera, bryozoans, fine-grained sandstone lithoclasts, limestone intraclasts, sand-to silt-size quartz grains and oolites (Fig. 8C-D). Some micritic intraclasts show inclusions of authigenic quartz crystals and evaporite calcite pseudomorphs, suggesting precipitation of these authigenic crystals before re-sedimentation.

5.3.2. Interpretation

This lithofacies represent carbonate sand deposits formed in open sea under high hydrodynamic conditions. The mixed oolitic, skeletal and intraclast components represent resedimented material from shallower reefal and oolitic factories, outer platform or older sedimentary rocks (e.g. sandstone lithoclasts). The lithosomes with large-scale planar to sigmoidal cross bedding are interpreted as energetic bars deposited in a middle ramp/platform and prograding basinward from avalanche of sediment. The channel-like beds may represent the infill of channels and gullies cutting the slope, where high-energy currents, which might have been induced by storms or slope instability, transported sediments from shallower areas.

5.4. Lithofacies F4: brachiopod and oyster beds

5.4.1. Description

They consist of 0.15–7.5 m thick lumachela beds of brachiopod and oyster shells. The beds exhibit a rudstone-rudite texture with bioclastic marly matrix. The majority of the specimens are articulated and display complete valves, suggesting minimal transport (autochthonous to parautochthonous deposits). The base and top of the beds are usually sharp, the base being occasionally erosive. These beds appear in three contexts: 1) as massive beds with erosive and channelized bases and with high density of specimens almost without sediment in between. These beds appear sharply interbedded between marls or calcarenites; 2) at the base and changing laterally to channelized oolitic and skeletal grainstones, and 3) on top of channelized grainstones and progradational grainstone bars and deltaic sequences.

5.4.2. Interpretation

Brachiopods were epifauna growing probably in relatively deep and quiet waters where they grew relatively quick and attached to firm substrates. Those beds with erosive and channelized bases are interpreted to have been deposited from gravity-driven sediment flows and are interpreted as debrite levels with little transport. Those beds with non-erosive bases developed on top or laterally to migrating grainstone bars are interpreted as autochthonous accumulations and clusters developed on abandoned bars or in interbar areas.

5.5. Lithofacies F5: sponge wackestone

5.5.1. Description

This is a minor lithofacies that consists of decimetric, tabular to nodular limestone beds made of dark micrite with dense

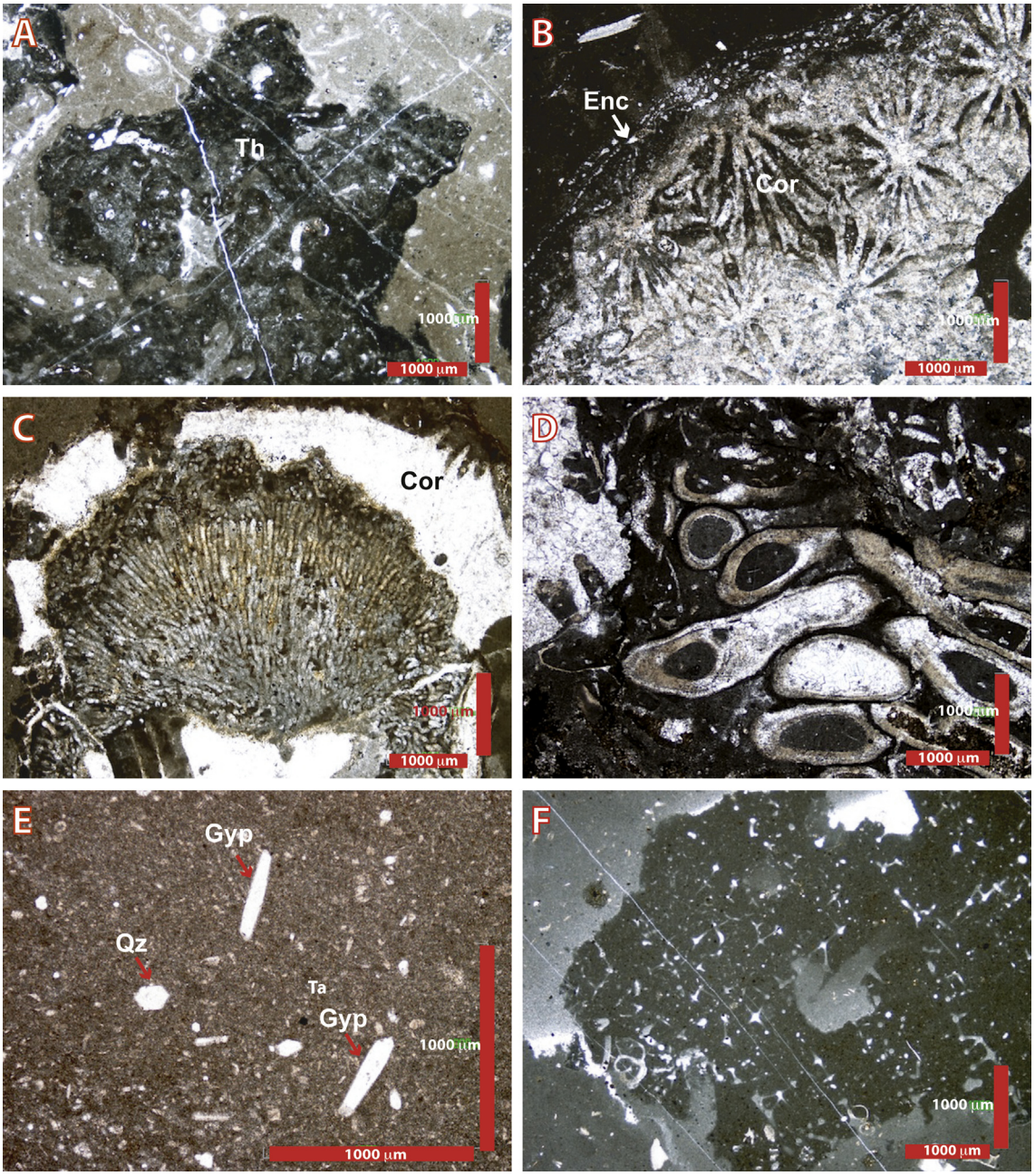

Fig. 7. Thin section photo-micrographs characterizing different microfacies types present in the reefal facies of the Azag minibasin. (A) Thrombolitic (Th) microbialite crust; (B) Coral (Cor) with incrusted micro-organisms (Enc); (C) Cryptobiontic *Rivulariacean*-type filamentous cyanobacteria inside a coral cavity (Cor); (D) Colony of serpulids (worm-tubes) in inter-coral spaces; (E) Early authigenic quartz (Qz) and pseudomorphs after gypsum (Gyp) embedded in micrite matrix; (F) Hexactinellid sponge wackestone.

population of sponges. Limestone beds stack in packages up to 2 m thick that appear below and grade laterally updip to lithofacies F1. In thin section, the microfacies consists of bioclastic wackestones with well-preserved siliceous sponges. Both desma-bearing demosponges (lithistids) and hexactinellid sponges have been recognized (Fig. 7F). The micrite matrix between the spongy bodies includes a variable amount of peloids, echinoderm debris and spines, bivalve shell fragments, rare benthic foraminifera, gastropods and coral debris.

5.5.2. Interpretation

This lithofacies is interpreted as a sub-photic benthic community. The co-occurrence of hexactinellid and lithistid sponges was common during the Mesozoic, although the hexactinellids tended to occur in deeper waters than the lithistids (Crevello and Harris, 1984; Rosales et al., 1995). This lithofacies suggests deposition under quiet paleoenvironmental conditions and low sedimentation rates downslope of the coral facies, in a reef slope where bottom currents became loaded with organic material and nutrients for feeding (Rosales et al., 1995).

5.6. Lithofacies F6: lithoclastic-bioclastic rudstone, carbonate breccia and pebbly marl

5.6.1. Description

It consists mainly of coral rubble and limestone blocks up to

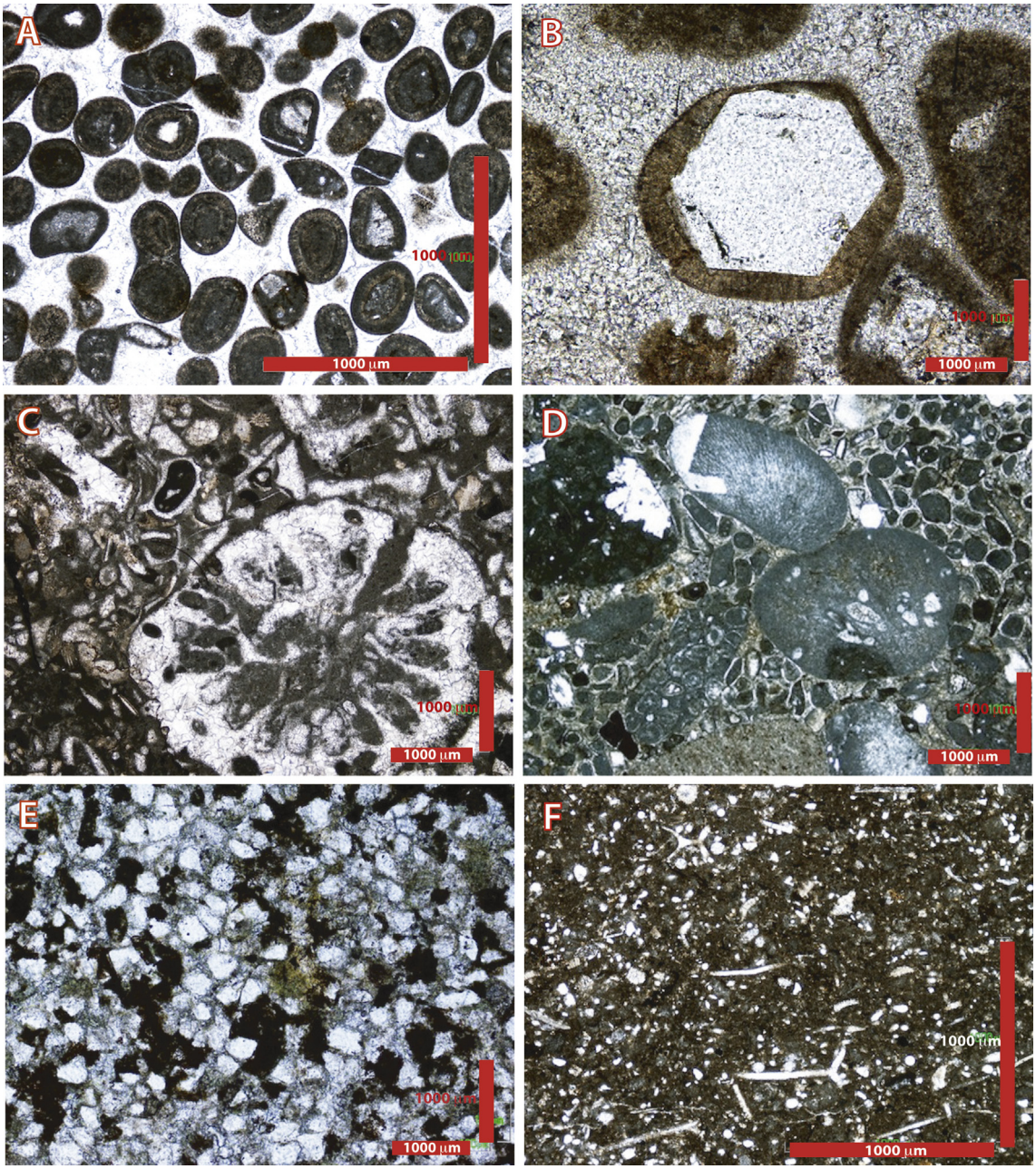

Fig. 8. Thin section photo-micrographs characterizing different microfacies types present in the Azag minibasin. (A) Oolite grainstone with simple and composite ooids; (B) Ooid with a nucleus of idiomorphic authigenic quartz; (C) Skeletal packstone with coral fragments; (D) Mixed skeletal-intraclast-oolite grainstone; (E) Fine-grained quartz-wacke with detrital coal fragments; (F) Spiculitic wackestone with monoaxon and triaxon sponge spicules.

30 cm long, embedded in a marly matrix along with a mixture of unsorted bioclasts including bivalves, belemnites, inoceramids, brachiopods, echinoids, crinoids and others. Beds are massive and irregular, 0.25–7 m thick. The fabric ranges from clast-to mud-supported breccia to marl with dispersed coral cobbles and limestone clasts. This lithofacies is locally associated to slumped beds.

5.6.2. Interpretation

This lithofacies is interpreted as platform-derived material transported to downslope environments by gravitational processes such as grain flow, debris flow and rock fall.

5.7. Lithofacies F7: bioclastic marls and marly calcarenites

5.7.1. Description

This lithofacies consists of 0.10–2 m thick beds of bioclastic marls and muddy, fine-grained calcarenites. The beds are massive, usually lacking lamination or grain gradation, and are bioturbated. The bases are sharp to slightly erosive. Allochems include soft muddy pebbles, limestone intraclasts, brachiopods and remains of crinoids, bivalves, oysters and rarely corals and serpulids.

5.7.2. Interpretation

These beds are interpreted as muddy debrites deposited from mass gravitational flows including mud-flow and debris-flow

processes.

5.8. Lithofacies F8: interbedded sandstones, siltstones and shales

5.8.1. Description

This lithofacies consists of heterolithic siliciclastic lithologies made of claystones and marly shales interbedded with thin-bedded sandstones and siltstones, and cross-bedded sandstones. Thin-bedded sandstones and siltstones are few centimeters up to 0.15 m thick and show erosive bases, normal grain gradation and ripple cross-lamination at the top. Cross-bedded sandstones consist of up to 0.5 m thick beds of fine-grained greywackes with coal detritus (Fig. 8E), current ripple cross-lamination and bioturbation. The sandstone beds stack in packages up to 5 m thick. These lithologies appear organized in coarsening- and thickening-upward sequences 10–60 m thick, showing a gradual transition from claystone with scarce thin-bedded siltstones and sandstones, to packets of cross-bedded sandstones.

5.8.2. Interpretation

The thin-bedded siltstones and sandstones are interpreted as siliciclastic turbidites interbedded in muddy facies of prodelta environments, whereas the packets of cross-bedded sandstones represent sandier facies of the delta front or deltaic bars. Thus, the coarsening- and thickening-upward siliciclastic sequences suggest progradation of delta lobes showing a transition from muddier prodelta facies into delta front environments.

5.9. Lithofacies F9: marls and marly limestones

5.9.1. Description

This lithofacies is characterized by thick successions (up to 120 m thick) of monotonous grayish marls and marly limestones with scarce bioclasts and belemnites. The bioclasts are composed mainly of centimeter-sized debris of bivalves, brachiopods, echinoids and oysters.

5.9.2. Interpretation

This lithofacies is interpreted to have been deposited in low energy, basinal to outer platform environments.

5.10. Lithofacies F10: marls with thin-bedded siltstones and calcisiltites

5.10.1. Description

It consists of a heterolithic lithology made of marls and marly limestones with intercalated thin, sheet-like beds of horizontal and ripple-laminated siltstones and calcisiltites. The siltstone and calcisiltite beds are usually 0.5–5 cm thick, and display sharp bases and grain gradation, occasionally with wavy to ripple cross-lamination at the top. This heterolithic facies conforms thick successions up to 30 m thick dominated by the muddy lithology, and where the thin-bedded siltstones and calcisiltites appear at irregular intervals of several meters to about 0.20 m.

5.10.2. Interpretation

The absence of thinning or thickening-upward trends and the dominant muddy nature of this facies suggest a basinal environment below the storm wave base, where the muddy lithology represent the basinal background sedimentation and the intercalated sheet-like thin beds represent diluted siliciclastic and carbonate turbidites. These turbidites were deposited from low-density turbidity currents, which may have been triggered by storms (distal tempestites) or slope instability.

5.11. Lithofacies F11: black lime mudstones

5.11.1. Description

This lithofacies consists of decimetric (0.20–0.50 m thick) tabular beds of black to dark grey lime mudstones. The beds are organized in thickening-upward packages up to 54 m thick. Bioturbation is rare and consists of *Chondrite* traces. Bioclasts are also scarce and include thin bivalve shells. The microfacies consists of a mudstone to wackestone texture with some debris of echinoderms and thin-shelled bivalves and sponge spicules. Framboidal pyrite and pyrite nodules and cubes are widespread.

5.11.2. Interpretation

The difference in the color (black) of this limestone lithofacies compared to other lithofacies of the Azag minibasin may be due to deposition in a poorly oxygenated sea floor and to a higher amount of organic matter and pyrite content. The low diversity of ichnotraces, which are dominated by *Chondrites,* suggests restricted conditions within the area of deposition and also poorly oxygenated bottom waters (Bromley and Ekdale, 1984). Further evidence of low-oxygen bottom-sea conditions are the abundance of pyrite framboids, which were most likely derived from aqueous sulphide via the activity of sulphate-reducing bacteria during early stages of diagenesis and under oxygen-deficient bottom-sea conditions (Wilkin and Barnes, 1997; Wignall et al., 2005). A possible cause for the anoxic conditions governing the sedimentation of these black mudstones is that the Azag was during this time a silled minibasin with very limited deep-water circulation.

5.12. Lithofacies F12: spiculitic-silty marls and limestones

5.12.1. Description

It consists of very fine-grained calcarenites, calcisiltites and marls. Beds are few decimeters up to 0.60 m thick and are organized in packets up to 6 m thick of stacked tabular to nodular beds. In thin section the texture is made of wackestone to packstone rich in monoaxon and triaxon sponge spicules (Fig. 8F). Other components are silt-sized quartz grains, peloids, debris of echinoderm and thin-shelled bivalves, ostracods, rare small benthic foraminifera and scarce coral and oyster debris. Pyrite in framboids and cubes may be abundant.

5.12.2. Interpretation

This lithofacies is interpreted to represent deposition in open-sea, calm outer platform environments with some siliciclastic influence. Lithofacies F12 appears usually associated to lithofacies F9 and F11.

5.13. Lithofacies F13: rhythmic bedded and nodular marls and limestones

5.13.1. Description

This lithofacies consists of rhythmically bedded limestone-marl sequences up to about 110 m thick. Individual limestone beds display thickness ranging between 0.10 and 0.30 m, whereas the marlstone beds are 0.20–2 m thick. Ammonites, belemnites, plant fragments and *Cancellophycus (=Zoophycus)* fossil traces can be present.

5.13.2. Interpretation

This lithofacies is interpreted to represent deposition in hemipelagic, outer ramp environments.

5.14. Lithofacies F14: ferruginous crust

5.14.1. Description

This is a minor lithofacies characterized by the presence of a localized iron crust with thickness ranging from 2 to 10 cm and slightly irregular morphology. Incorporated in the crust a dense accumulation of well-preserved ammonites and belemnites is observed. In thin-section the crust exhibits ferruginous microstromatolite layers with encrusting foraminifera and serpulids.

5.14.2. Interpretation

The iron-crust surface represents a discontinuity surface with associated condensation and hardground development. Under such as conditions, processes related to the activity of iron-oxidizing microbial communities can be responsible for the stromatolite formation and Fe mineralization (Préat et al., 2000; Jakubowicz et al., 2014). The consortium of ferruginous stromatolites, serpulids and encrusting foraminifera is a common feature of many Mesozoic hardgrounds and condensed sections of the Tethyan realm (e.g. Di Stefano and Mindszenty, 2000; Préat et al., 2000; Reolid et al., 2008; Najarro et al., 2011).

6. Stratigraphy and facies architecture

The sedimentary infill of the Azag minibasin shows a general tilting to the west, with the base of the stratigraphic section being exposed in the eastern basin margin (Fig. 5). The sedimentary pile thins to the southern and to the northern exposed margins, where wedges of growth strata and abundant shallow marine carbonate lentils (lithofacies F1, F2 and F3) developed. To the west, the basin ends plunging towards the Tillicht thrust weld (Fig. 9a).

A complete stratigraphic section of the upper Lias to Bajocian-p.p. Bathonian? deposits of the Azag minibasin is represented in Fig. 10. Including the lower Liassic rocks, 10 stratigraphic units have been recognised and are represented in the geological map and in the structural and stratigraphic profiles (Units I to X; Figs. 3, 5 and 6), based on observable lithological changes with cartographic identity, the existence of unconformities and stratal geometries marking significant changes in the basin evolution. A correlation of the central reference section with the reduced successions of the basin margins is shown in Fig. 11. For the lower part of the succession the units distinguished (Units I and II) coincide with previous formally defined lithostratigraphic units (Idikel and Ouchbis Formations, Hettangian?-Sinemurian to Pliensbachian; Studer, 1987). For the rest of the section (Toarcian to Bajocian-p.p. Bathonian?) an informal stratigraphic schema for the Azag minibasin is proposed here (Units III to X), including a correlation attempt with the previously published stratigraphic framework of the central High Atlas (Table 1, Fig. 3).

6.1. Unit I

Unit I corresponds to the Idikel limestone and dolomite Formation (Studer, 1987; redefined by Mehdi et al., 2003), which is exposed in the eastern margin of the Azag minibasin. There, the Idikel Formation is thin (less than 90 m), due to tectonic lamination against the welded salt wall. In contrast, in the hanging wall of the Jebel Tillicht anticline (Foum Tillicht section, Wilmsen and Neuweiler, 2008) the whole Idikel Formation has a total thickness of 240 m, and is described as formed by massive black dolomite and limestone beds with shallow marine facies assemblages. The age of the Idikel Formation is Hettangian?–lower Sinemurian according to Wilmsen et al. (2002) and Mehdi et al. (2003).

6.2. Unit II

Above the limestones and dolomites of the Idikel Formation, a regular hemipelagic rhythmite of light-coloured limestones and marls with an average bed thickness of 10–40 cm occurs conforming the Unit II. This unit corresponds to the Ouchbis Formation of Studer (1987). No facies belonging to the Foum Zidet Formation (Upper Sinemurian; Mehdi et al., 2003) have been identified in the Azag minibasin. In contrast, in the western side of the Jebel Tillicht thrust weld (Jebel Idirht and Jebel Amalou Tassalaht) this latter formation is well developed, including spectacular sponge bioconstructions (Neuweiler et al., 2001 and references herein). In the eastern margin of the Azag minibasin, the Ouchbis Formation (Unit II) reaches a maximum thickness of about 120 m that decreases to the south in outcrop. It is much thinner compared to the neighbouring Foum Tillicht section, where it attains up to 300 m (Wilmsen and Neuweiler, 2008). The ammonite *Taurameniceraselisa* (Fucini) (A. Goy pers. com.) has been collected from the upper part of the Ouchbis Formation, which characterizes the Spinatum Zone/Hawskerense Subzone of the Upper Pliensbachian. Thus, a Pliensbachian age is assigned to Unit II.

6.3. Unit III

The Ouchbis Formation is sharply overlain by marls and nodular marly limestones (lithofacies F9) of the Unit III. This sharp transition may correspond to the drowning unconformity recognised on top of the shallow marine Pliensbachian platforms in the southern margin of the Atlas Basin (Wilmsen and Neuweiler, 2008), as well as in the eastern Djebel Bou Dahar block (Merino-Tomé et al., 2012). Unit III is a thin unit representing relatively low sedimentation rates, which ends with a ferruginous hardground of regional extent (lithofacies F14) (Sadki, 1992). In the measured logs, the total thickness of Unit III ranges between 65 and 110 m (with a maximum of 200 m along section 6a, Fig. 6), which is lower than in the neighbouring units of Foum Tillicht and Rich, where it exceeds 330 m (Bodin et al., 2016; Sadki, 1992, 1996; Ait Addi and Chafiki, 2013). The lower part (subunit IIIa) is up to 45 m thick, and is constituted by light-coloured marls with scarce thin beds of fine-grained nodular limestone (lithofacies F9), and by dark shales with interlayered fine-grained siliciclastic turbidites (lithofacies F10) (Fig. 9b). This part of the section corresponds to the Tagoudite Formation of Studer (1987), and its age is lower Toarcian (Studer, 1987; Wilmsen et al., 2002). This change from marl-carbonate deposits to clays and siliciclastic turbidites may reflect the impact of the early Toarcian Anoxic Event (T-OAE) in the basin, as documented in other areas of the central High Atlas (Bodin et al., 2016). The upper part of Unit III (subunit IIIb) is made of nodular marls and limestones that alternate with thin beds of grey marls and limestone (lithofacies F9) and thin intercalation of fine-grained siliciclastic turbidites (lithofacies F10). The succession ends with alternating layers of grey marls and micritic limestones that include *Cancellophycus* in the upper part. Finally, the succession is capped by a well-developed hardground at the top of Unit III.

Ammonites of the Middle Toarcian (Phymatoceratinae: *Brodieia*/*Merlaites*, Gradata Zone), of the Upper Toarcian [*Pseudogrammoceras* cf. *fallaciosum* (Bayle), of the upper part of the Bonarelli Zone and interval Zone between Speciosum and Meneghini], and of the Aalenian [*Brasilia similaris* (Buckman), Murchinsone Zone, Bradfordensis Subzone] have been found in this unit (A. Goy pers. com.). Along the topping hardground, the encountered ammonite fauna includes *Ambersites aegratus* Buckman (Murchinsone Zone, Bradfordensis Subzone) and *Haplopleuroceras* cf. *subspinatum* (Buckman) (Concavum Zone) from the Aalenian, and piritic nuclei of *Hyperlioceras* sp. (Lower Bajocian, Discites Zone) and *Bradfordia*?

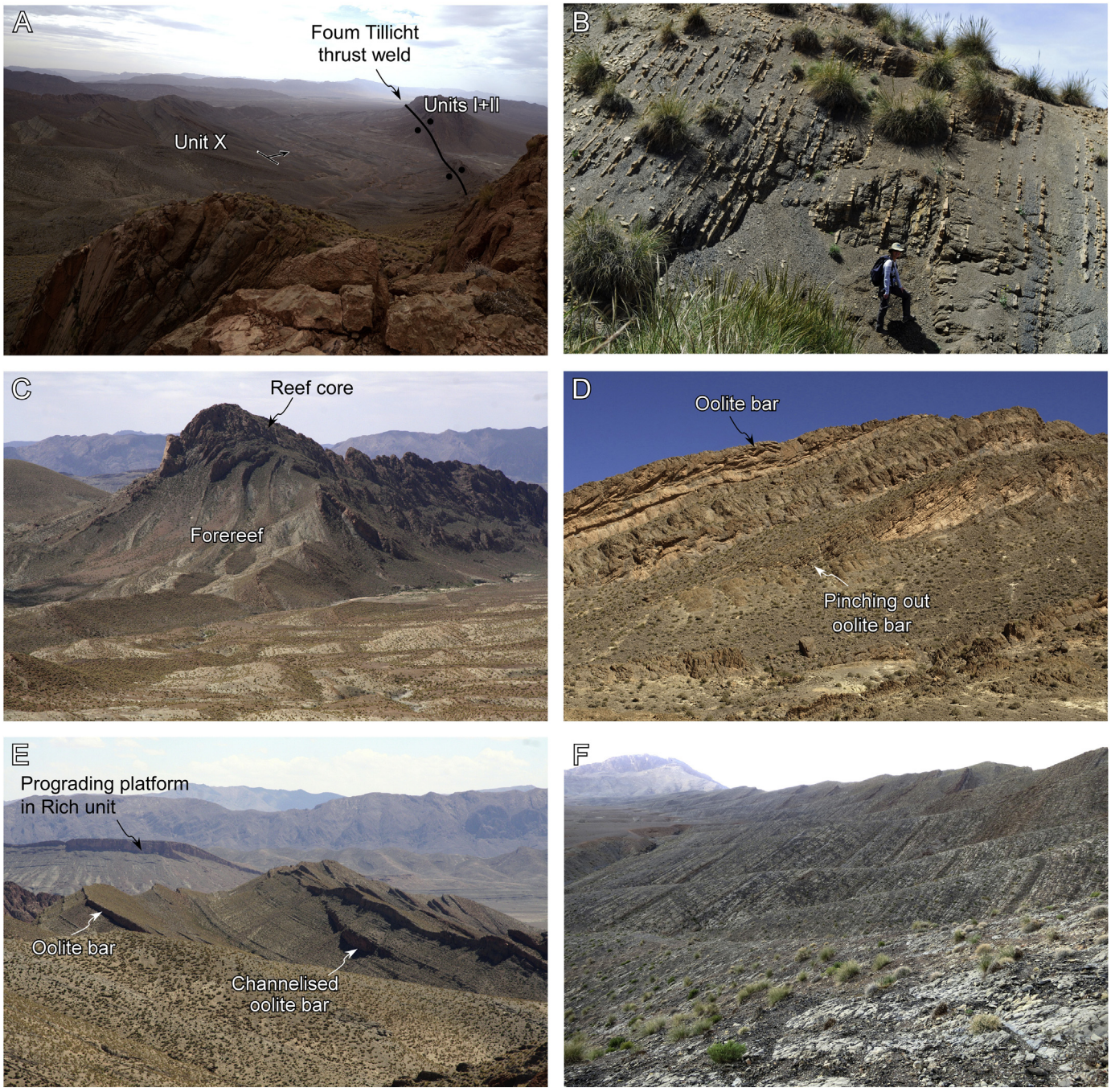

Fig. 9. Field photographs of the Azag minibasin infill. (A) View of the western side of the basin showing west-dipping shale and limestone beds of unit X, which abut against the western weld bounding the minibasin; (B) View of the Toarcian shale and sandstone layers of unit III, eastern side of the minibasin; (C) The southern reef passing to reef slope deposits viewed from the north (unit V). Field of view is approximately 500 m. Bedding is vertical to steeply west-dipping. (D) View of cross-bedded oolite bars near the southern basin margin (unit VIII); (E) View of the west-dipping central part of the Azag minibasin looking south; (F) View of west-dipping dark lime mudstone layers of unit IX.

sp., *Witchellia*? sp., *Maceratites*? sp., *Lissoceras*? sp., *Phylloceras* sp. and *Lytoceras* sp. from the interval Aalenian (Concavum? Zone) to Bajocian (Laeviuscula? Zone) (A. Goy pers. com.). Therefore, an early Toarcian to late Aalenian age is deduced for Unit III.

6.4. Unit IV

The hardground on top of Unit III is overlain by Unit IV in onlap to an apparent southward direction (Fig. 5). Unit IV consists of a thick growth strata succession (210 m in the measured log of Fig. 10, up to 600 m in the section of Fig. 6a) of predominantly light-coloured marls. In the lower part (first 45 m) it is made of lithofacies F9 with marly limestone intercalations, whereas in the upper part it contains sequences of lithofacies F9 at the base grading upward to lithofacies F10 with scarce thin-bedded, fine-grained siliciclastic turbidites. The top of unit IV is marked by a gentle angular unconformity and the sharp appearance of a reef in the southern basin margin. At the base of unit IV, the ammonites *Otoites* sp. (cf. *pauper* Westermann/*delicatus* Buckman), *Otoites fortis* Westermann, *Phylloceras* sp. and *Lytoceras* sp. (lower Bajocian, Laeviuscula Zone –Sauzei Zone) have been found. 7 m above the hardground the ammonites found were *Otoites* cf. *contractus*

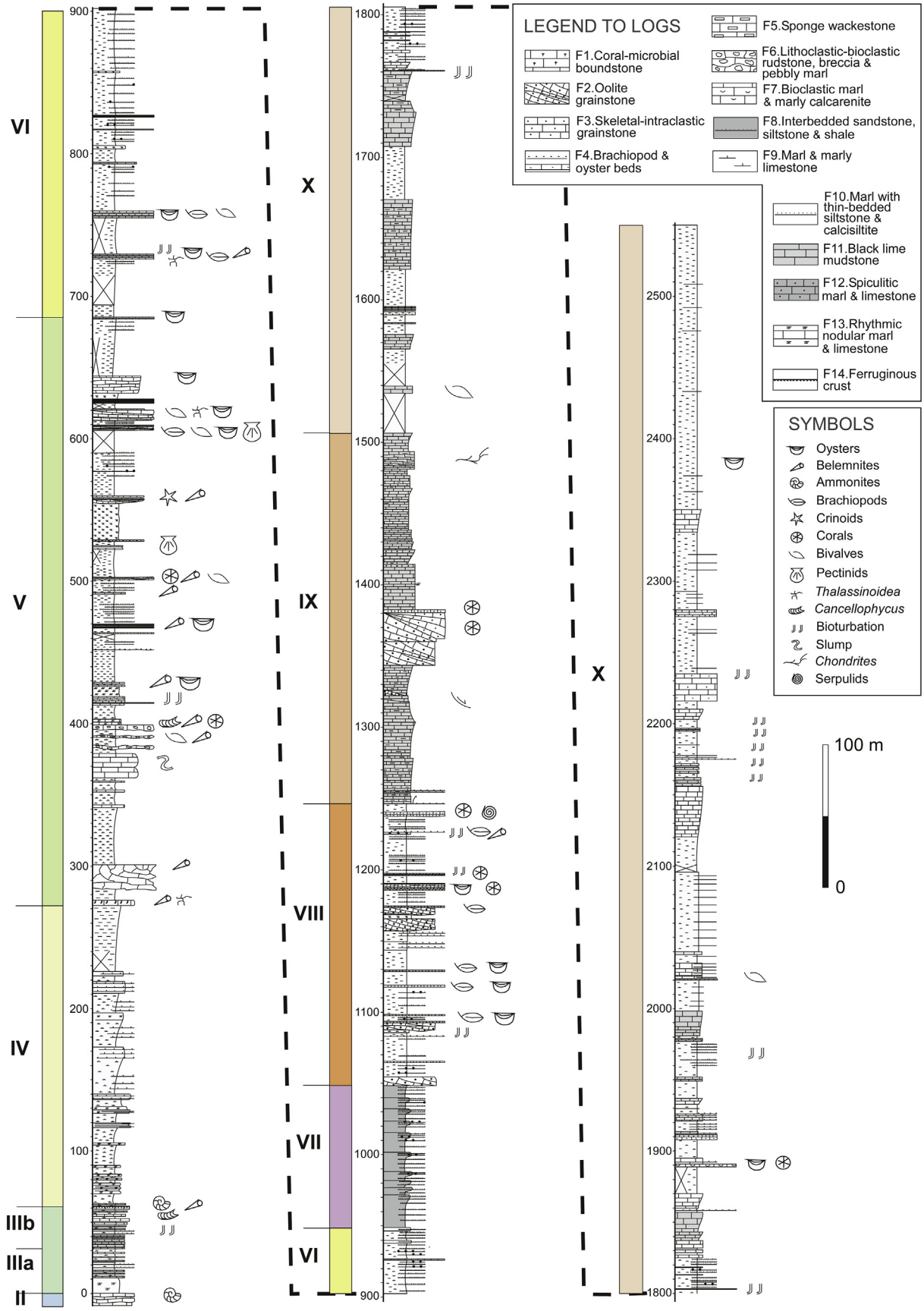

Fig. 10. Detailed stratigraphic section of the Toarcian to Bajocian-Bathonian? infill of the Azag minibasin. The location of this profile is shown as 2 in the inset map of Fig. 11.

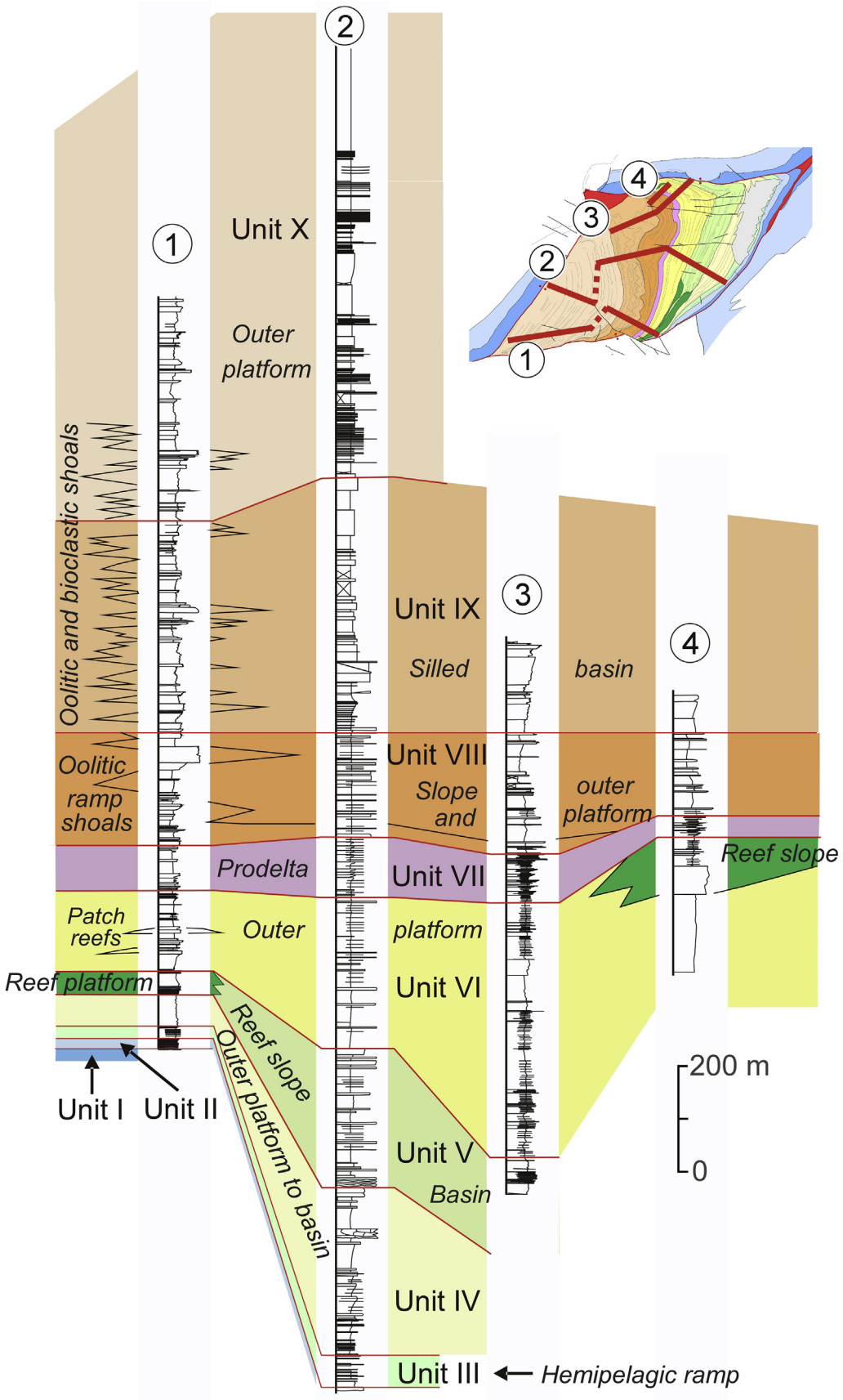

Fig. 11. Correlation panel of stratigraphic logs of the Azag minibasin showing thickness variations of the different units as measured in the field.

(Sowerby) and *Hebetoxytes* sp. (lower Bajocian, Laeviuscula Zone –Sauzei Zone). On the basis of the ammonites collected and on the stratigraphic position, an early Bajocian age is attributed to this unit.

6.5. Unit V

Unit V is characterized by the development of a coral reef build-up in the southern basin margin and their age equivalent fine-grained facies into the basin (Figs. 9c and 12). Strata of the reef lithofacies (F1) are now in vertical attitude and up to 130 m thick, whereas the equivalent slope and basinal facies are represented by a 415 m-thick measured succession of marls, marly limestones, thin layers of fine grained turbidites, and reef-derived slumps, breccias, debrites and calcarenites (lithofacies F10 and F6). In the lower part of the unit the background basin sedimentation corresponds to marls and marly limestone (lithofacies F9) whereas in the middle and upper part of the succession it changes to lithofacies F10 that includes scarce thin-bedded siliciclastic turbidites. The reef-derived sediments are slumps and coarse breccias in the lower part turning into debrites and calcarenites in the upper part. This vertical facies evolution composes a marked growth strata fan and coincides with a mainly aggradational pattern of the reef margin, which ends with a huge sheet of bioclastic calcarenites expanding basinwards (Fig. 12). *Cancellophycus* is still present in the middle part of Unit V. Ammonites from the lower Bajocian (*Skirroceras* cf. *macrum* (Quenstedt) and *Skirroceras* sp., upper part of the Sauzei Zone and the Humphresianum Zone, A. Goy, pers. com.) have been collected in the upper half of unit V. Thus, an early Bajocian age is assigned to the unit.

6.6. Unit VI

The basal contact of Unit VI is defined by a flooding surface over the southern coral reef build-up and associated facies. The unit consists of a thick sequence (up to 520 m) of marls with thin-bedded fine-grained siliciclastic turbidites, which become progressively more abundant upwards (lithofacies F10). Bioclastic debrites (lithofacies F7) are abundant in the lower part of the unit while siliciclastic influx is scarce. In the upper part of the section the bioclastic debrites become thinner and sparse. This unit is related to a renewed reef growth, in this case in the northern margin of the Azag minibasin (Fig. 13). In the southern margin some small patch reefs still persisted in the lower part of the unit attached to the basin margin. An early-late Bajocian age is tentatively assigned to this unit.

6.7. Unit VII

Unit VII is defined by an increase of siliciclastic influx and a marked colour change in the field. It consists of up to 10 thickening- and coarsening-upward sequences of shales and siltstones with abundant thin layers of fine-grained siliciclastic turbidites (lithofacies F8). The total thickness of the unit is over 100 m. In the upper part of the unit the siliciclastic turbidites become thicker, up to 10 cm, with a well-developed Bouma Ta-c sequence. These sequences are interpreted in this work as the progradation of distal deltaic lobes that filled the basin, although equivalent turbiditic layers to the south of the Azag minibasin near Rich were interpreted by Ait Addi (2008) as tempestites. To the northwest of the Azag basin, Brechbühler et al. (1988) reported the presence of abundant siliciclastic turbiditic deposits of western provenance in a similar stratigraphic position. This unit represents the progradation of a distal deltaic depositional system (prodelta, Fig. 11) that post-dated the stage of reef development on the northern basin margin. To the north it wedges out onto the reefal growth strata (Fig. 6b). On the basis of its stratigraphic position, a late Bajocian age is suggested for this unit.

6.8. Unit VIII

Unit VIII represents a return to dominant carbonate sedimentation. It starts with the sudden apparition of prograding oolitic bars (lithofacies F2 and F3, Fig. 9d and e) into the basin from a south and south-eastern provenance. Between the oolitic bars are marls and occasional marly limestones with abundant bioclastic debrites (lithofacies F7). Coral debris and small patches of *in situ* coral growth are abundant in the upper part of the unit. To the northern basin margin the oolitic bars pinch out and disappear between marls, and are rapidly replaced updip by wedges of cross-bedded bioclastic grainstones (lithofacies F3) that overlap the northern ridge (Fig. 13). The bioclastic and coral debris provenance of these latter calcarenitic bars is probably from a northern reef development, now eroded. Debrites are thicker and more abundant in the northern sections, where wedges of prograding mixed calcarenites (lithofacies F3) also developed. The recorded thickness of unit VIII is close to 200 m, and it is probably equivalent to the unit D of Stanley (1981) defined in the neighbouring basin of Rich. Unit VIII is probably equivalent to the oolite-rich Assoul Fm. defined for the Amellago platform area, SW of the study area (Christ et al., 2012). Unit VIII is attributed to the late Bajocian.

6.9. Unit IX

Unit IX is defined by an abrupt change in the background basin sedimentation. Dark marly limestones and micritic limestones (lithofacies F11) are the dominant lithofacies of the unit (Fig. 9f), with scarce influx of fine-grained bioclastic calcarenites (lithofacies F7, F12). In the middle of the unit some thick oolitic bars with south-eastern provenance still exist, with microbialite-coral patch reef development on their tops. The total thickness of this unit is about 260 m. To the north, this unit represents the end of the shallow water carbonate sedimentation, fossilizing the residual relief of the reef-related calcarenitic bars at the basin margins. Compared to areas outside the Azag minibasin, this unit could be partly equivalent to the classic “Calcaire Corniche” of Du Dresnay (1971), and may be attributed to the late Bajocian.

6.10. Unit X

Unit X consists of interbedded marls and marly limestones (lithofacies F9 and F12) and dark micritic limestones (lithofacies F11) as the background basin sedimentation. In the upper part the section is marly-dominated, with scarce colonies of oyster shells (lithofacies F4). Marginal grainy carbonate facies (lithofacies F3) are well developed, especially in the southern margin, but very restricted to the vicinity of the edge of the margin (Fig. 11). At the southern margin, back-stepped thick oolitic limestone bars also occur, with small coral patch reefs (lithofacies F1) developed on their tops. In the rest of the section and in the northern margin, the marginal carbonate wedges are made by hybrid (mixed) calcarenites (lithofacies F3). In the central part of the basin these grainy facies are restricted to thin calcarenitic beds and sparse very thin layers of calcareous turbidites (lithofacies F10). The total thickness of this unit is about 1050 m; the marly-dominated part corresponds to the upper 270 m. In the absence of representative fauna, according to its stratigraphic position Unit X could be tentatively attributed to the late Bajocian-early Bathonian?

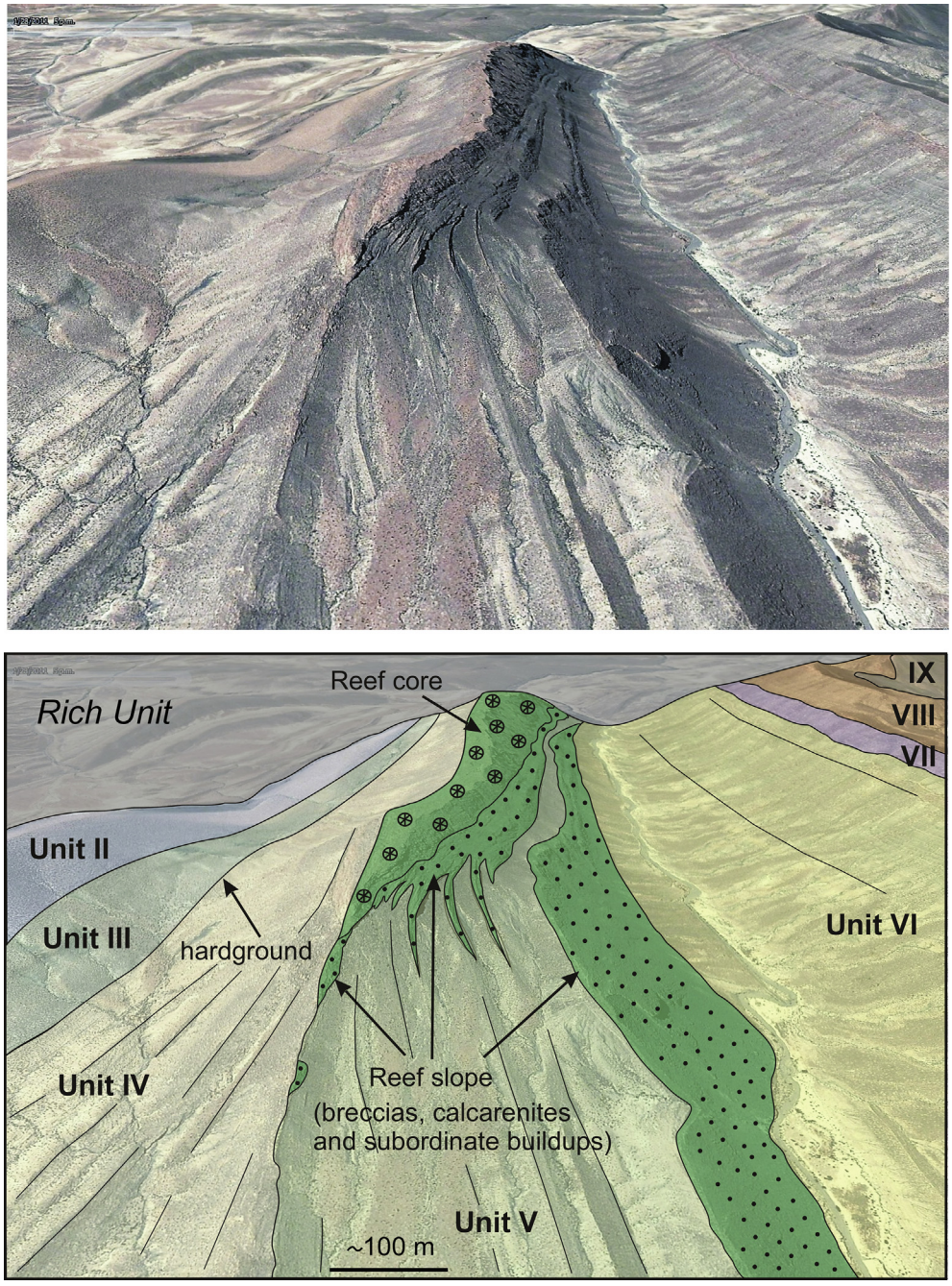

Fig. 12. Google Earth oblique view of the northern margin of the southern reef system, viewed from the north. The geometry of the southern end of each aggradational parasequence, in the transition between the reef slope facies to the basin marls, conforms to the wedge halokinetic sequence pattern as defined by Giles and Rowan (2012).

7. Discussion

The Azag minibasin and flanking salt walls evolved within a rifting regime during the time recorded by the Jurassic deposits described. Evidence for synsedimentary salt tectonics is provided by upturning of layers, thinning of stratigraphic units towards the highs of the minibasin margins, wedges of growth strata and erosional truncations of localized extent, and is consistent with other structures reported in the High Atlas by Saura et al. (2014). The E-W profile of the Azag minibasin shows a rollover geometry (Fig. 6a). The general stratal dip to the west suggests that the basin depocenter migrated in that direction, whereas the eastern basin margin was a salt anticline or salt wall with upturned beds that dip away in both sides ("megaflaps" in the sense of Rowan et al., 2016). It must be noted that listric faults and associated rollovers are not characteristic structures of the High Atlas Jurassic rift, where Triassic ridges are usually antiformal salt walls with outward-dipping layers where differential sediment loading has significantly contributed to diapiric growth and basin subsidence. This suggests that the asymmetry and tilting of the Azag minibasin infill was caused by progressive westward expulsion of the Triassic evaporite unit by a laterally-migrating depocenter axis (i.e. resembling an expulsion rollover, Ge et al., 1997). However, the migration of the depocenters of the carbonate-dominated Azag

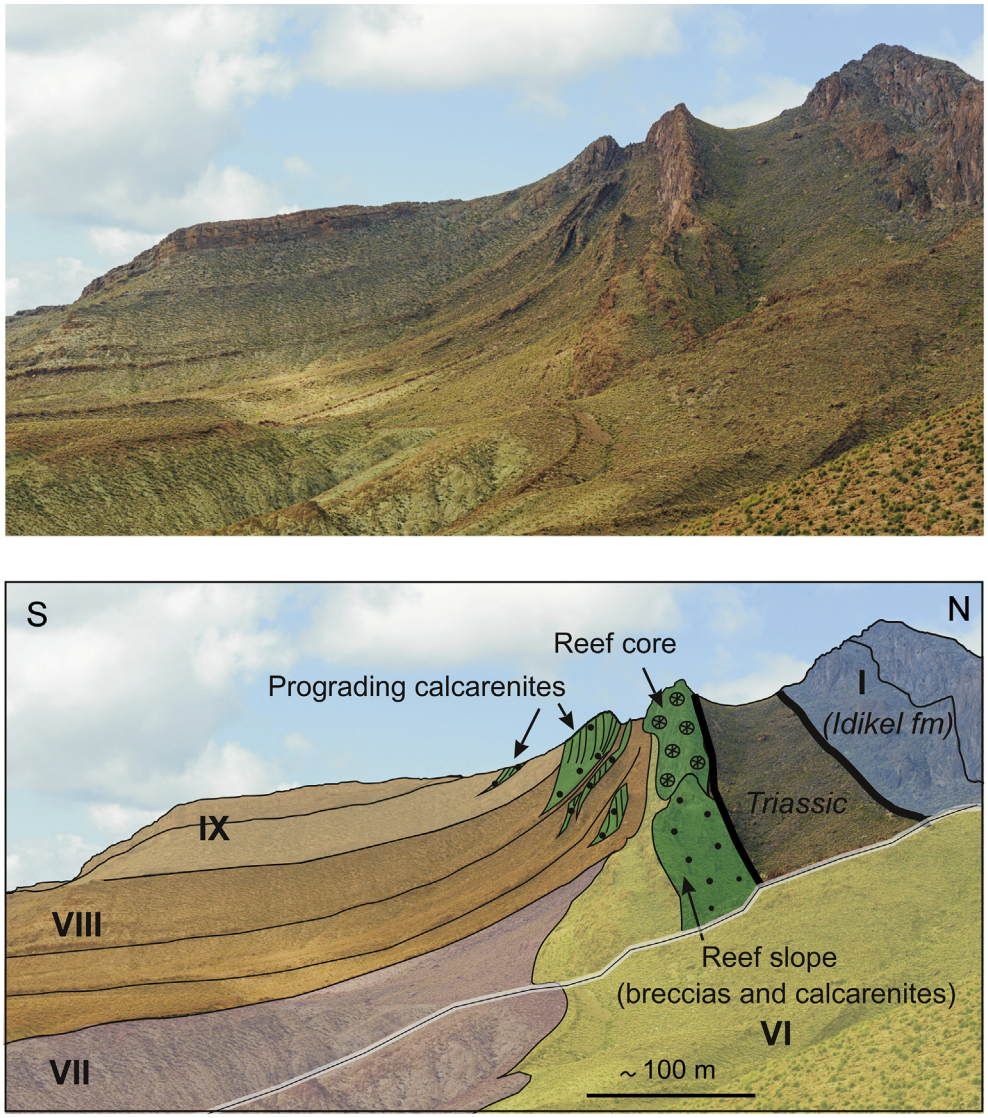

Fig. 13. Panoramic view of the northern reef margin of the Azag minibasin. The geometry is defined by the reef core and the reef slope calcarenites with a northern pinch out of basinal marls and debrites. The stacking pattern of the aggradational parasequences is akin to the wedge halokinetic sequence pattern as defined by Giles and Rowan (2012).

minibasin cannot be readily explained by the progradation of a clastic wedge as described by Ge et al. (1997). The causes of the laterally-varying salt expulsion, determining the shift of the minibasin infill, may reside in a preexisting relief or step of the base salt at depth, possibly in relation with a basement fault as tentatively depicted in Fig. 6a.

Tectonics and sedimentation relationships highlight the main steps in the evolution of the Azag minibasin. The minibasin infill is composed by a succession of varying stratigraphic units and facies assemblages that reflect localized spatial and time variations of accommodation within the basin that result from Triassic salt migration (salt evacuation in the basin depocenters, salt wall inflation in the margins), as well as from regional events that are approximately coeval in the whole Jurassic rift of the High Atlas. A similar dual control has been recently described in fluvio-lacustrine sediments of the Sivas Basin of Turkey in a recent work by Ribes et al. (2015), and is generally expected in other sedimentary basins influenced by the mobility of evaporites.

The halokinetic geometry of the Azag minibasin fill varies from unit to unit and from side to side of the basin, resulting in a marked basin asymmetry. Halokinetic strata as defined by Giles and Lawton (2002) and Giles and Rowan (2012) in the case of the La Popa basin of Mexico primarily record the relative rates of diapiric inflation and sediment accumulation in the margins of salt-controlled basins. Similarly, the asymmetric pattern of the Azag minibasin records spatial and temporal variations in diapir rise relative to sedimentation rates. Types of relationships observed at the Azag minibasin margins include: 1) gentle fans of growth strata bounded by apparent conformities or low-angle unconformities ("wedges" in the terminology of Giles and Rowan, 2012), which form during stages where the local sedimentation rate exceeded the diapir-rise rate, and 2) tabular, conformable packets that abut towards the basin margins at high angle ("T-shaped geometries" in Ribes et al., 2015) which formed in stages where the diapir-rise rate was balanced by the sedimentation rate. Hook geometries indicative of exceeding diapir-rise rates (Giles and Rowan, 2012) have not been observed.

The E-W section of the Azag minibasin provides little information for halokinetic sequence patterns adjacent to the bounding salt welds. A sequential evolution of the minibasin is best illustrated by

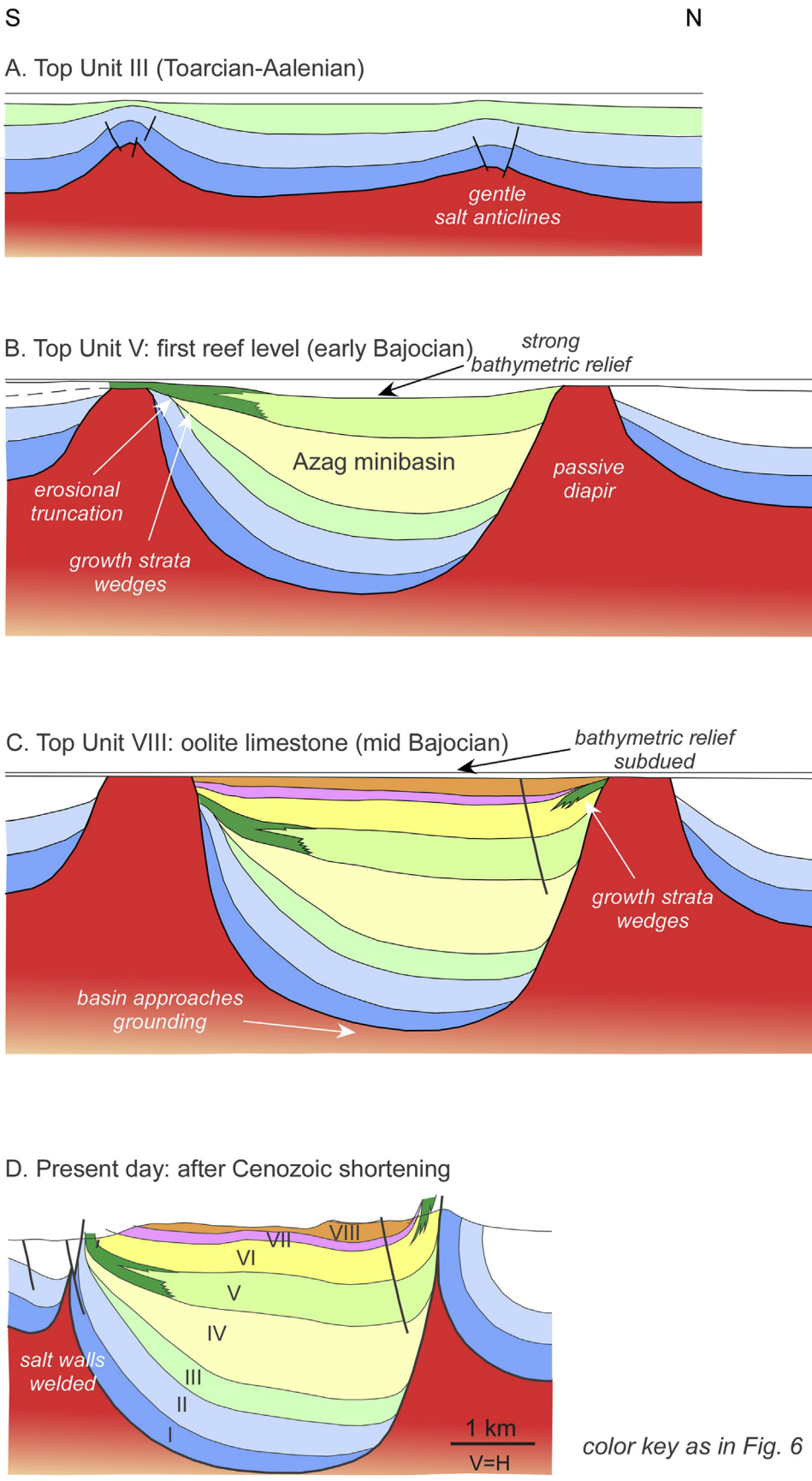

Fig. 14. Diagrammatic evolution though time of the Azag minibasin along a N-S profile. Sequential sections have been constructed using *Move* software. The original width of the salt walls enclosing the minibasin is unknown. See Fig. 5 for color key of stratigraphic units; no vertical exaggeration.

the N-S profile (Figs. 6b and 14) where the stacking pattern of stratigraphic units reflects varying processes through time. Moderate thickness variations in the Idikel and Ouchbis basal Formations in and out of the Azag minibasin are indicative of halokinesis initiating already in the Sinemurian-Pliensbachian. These formations show similar facies in the Azag minibasin and in the neighboring areas of the High Atlas, having been reported as post-rift transgressive deposits with respect to the Triassic rift episode (Laville et al., 2004), although contemporaneous low-strain normal faulting has been postulated (Wilmsen and Neuweiler, 2008; Lachkar et al., 2009; Merino-Tomé et al., 2012; Quiquerez et al., 2013). The cumulative thickness observed at their exposure in the eastern side of the basin is < 250 m, whereas in the adjacent margins of the Rich and Foum Tillicht basins they reach 700 m (Fig. 6). Only small thickness variations are observed in the N-S outcrop area of the Idikel and Ouchbis Formations within the Azag minibasin. Assuming that in the deep parts of the minibasin the thickness of these formations is comparable to that observed in the Rich and Foum Tillicht basins, we interpret that in the early Liassic the region was characterized by low-amplitude highs in between slightly more subsiding areas, namely a system of non-piercing salt anticlines or pillow-like structures overlapped by carbonate sedimentation (Fig. 14a). The causes for the initiation of salt migration in these early stages of overburden could have been linked to differential loading associated to underlying Triassic faults, or in association with incipient extensional faulting in the overburden itself, as illustrated by the small normal faults sealed by the Ouchbis Formation observed near the northern weld (Fig. 5). Only small differential loading is necessary to maintain low-amplitude halokinetic movements once differential subsidence is established by one of these mechanisms (e.g. Warsitzka et al., 2013, 2015).

The Pliensbachian-Toarcian transition is marked by an abrupt deepening of the basin and a change from carbonate to clastic sedimentation (shale and turbiditic sandstone, Unit III). This transition is recorded elsewhere in the High Atlas rift, and represents a roughly synchronous event of platform drowning in the rift axis and emersion in the rift margins, attributed to regional vertical movements coinciding with the early Toarcian eustatic high (Ettaki et al., 2000). The deepening profile actually starts with the transition from the Idikel shallow water to the deeper water carbonates of the Lotharingian-Pliensbachian formations, as happens elsewhere in the High Atlas of Rich (Neuweiler et al., 2001; Wilmsen and Neuweiler, 2008). Hence, variations in halokinesis cannot be invoked for the general trend of facies evolution of the Azag minibasin during these early Jurassic times, which rather reflects regional and global factors. Accumulation rates are still low for the Toarcian-Aalenian exposed in the Azag minibasin, although moderate thickness variations suggest the persistence of low-amplitude salt movements. From the Sinemurian to the Aalenian, the average (compacted) sediment accumulation rates observed in the Azag structure were <0.02 mm/yr. Sedimentation within this cycle terminates with a hardground of regional significance, that was also recognized in a diapiric high in the center of the Foum Tillicht unit (Bernasconi, 1983). Discontinuities in the interval between the upper Lias and the lower Bajocian are commonly reported in different sections of the Jurassic of the High Atlas (Du Dresnay, 1964; Sadki, 1992, 1996).

The Azag area records a major reorganization at the Aalenian-Bajocian boundary, which marks the onset of the main stage of downbuilding and full minibasin development. The remainder of the stratigraphic succession, which constitutes the bulk of the Azag minibasin infill (mostly Bajocian in age), records a dramatic acceleration of the (compacted) sedimentation rate during 4–5 Ma to an average of 0.6 mm/yr (0.5 mm/yr if the upper part is assumed to include the lower Bathonian). The Azag minibasin became a rapidly subsiding, west-migrating depocenter, whereas inflation of the salt walls at the northern and southern margins enclosing the minibasin is evidenced by stratal wedges and marginal reef complexes. The facies assemblages indicate that the Azag minibasin and adjacent salt walls were always submarine. Even if sediment accumulation in the Azag minibasin and elsewhere were partly accommodated by salt migration, regional extension and crustal thinning continued in the Atlas rift, as indicated by the contrast between the thousands meters of open marine deposits of Dogger age in the High Atlas and their inexistence in the present-day forelands north and south of the inverted rift.

The Bajocian-Bathonian? age of the main downbuilding phase in the Azag minibasin in the eastern part of the Central High Atlas compares well with a propagation sequence reported by Saura et al. (2014) for the western part of the central High Atlas. Bouchouata et al. (1995), Ettaki et al. (2007) and Moragas et al. (2016) reported a Liassic main age for the westernmost diapirs and basins (Izerki, Tazoult, Azourki), whereas more to the east, basins in the Imilchil area encompassed the late Liassic and the Dogger (Saura et al., 2014).

The late Aalenian-early Bajocian hardground is first covered by outer platform to basinal marl and marly limestone beds (Unit IV), which progressively onlap towards the southern margin of the basin and abut abruptly to the northern weld (Fig. 5). The strong asymmetry of Unit IV indicates contrasting salt inflation rates in the southern and northern salt walls. In the southern margin the unit defines a wedge where the sediment accumulation rate progressively exceeded the diapir-rise rate, whereas the more tabular T-shaped geometry of the northern margin indicate a higher diapir-rise rate, similar to the sediment accumulation rate. This asymmetry is maintained in Unit V, which defines a wedge in the south and a more tabular geometry in the north (Fig. 14b). However, sedimentary aggradation in the southern side was punctuated by episodes of non-deposition or erosion, coinciding with the hardground or at the base of unit V, which locally overlies the Ouchbis Formation (Fig. 15).

The coral reef of unit V probably topped the southern salt wall, and rapidly passed basinwards into deeper water shales and debrites, attesting for strong bathymetric relief (Fig. 13b). This situation is reversed for Unit VI, which shows a well-developed reefal and prograding platform complex in the northern side (Figs. 13 and 14b), indicating increased sedimentation rates in the northern margin of the Azag minibasin at that time. The northern reef is followed by an abrupt offlap, after which units VII and VIII exhibit onlapping wedges that attest for high sedimentation rates.

Evidence of diapirs exposed or lying near the sea floor at the Azag minibasin margins may be provided by the euhedral quartz and gypsum crystals in Units V and VIII, although passive diapirism may have likely started in earlier times during the strongly tapered Unit IV (early Bajocian). More compelling evidence for diapiric exposure is found in the northern side of the northern weld, near Jebel Tirrourdine (Fig. 16a), where the Toarcian?-Bajocian succession is in contact with the Triassic unit and with the weld itself. The map pattern at that locality is strongly suggestive of a larger diapir, trending obliquely to the main salt wall, that was flanked by the Idikel and Ouchbis Formations and whose top was overlapped by Toarcian?-Bajocian sediments. The diapir later fell so the topping sediments collapsed to weld down to the salt wall core, producing a map geometry similar to seismic profiles of fallen diapirs in the continental margin off Angola (Duval et al., 1992) (Fig. 16b). A triangular-shaped diapir was left in the eastern side in the Moroccan example, adjacent to which the Toarcian?-Bajocian sediments show a series of halokinetic unconformities attesting for the rapid diapir fall.

The salt wall tops may have been episodically overlapped by

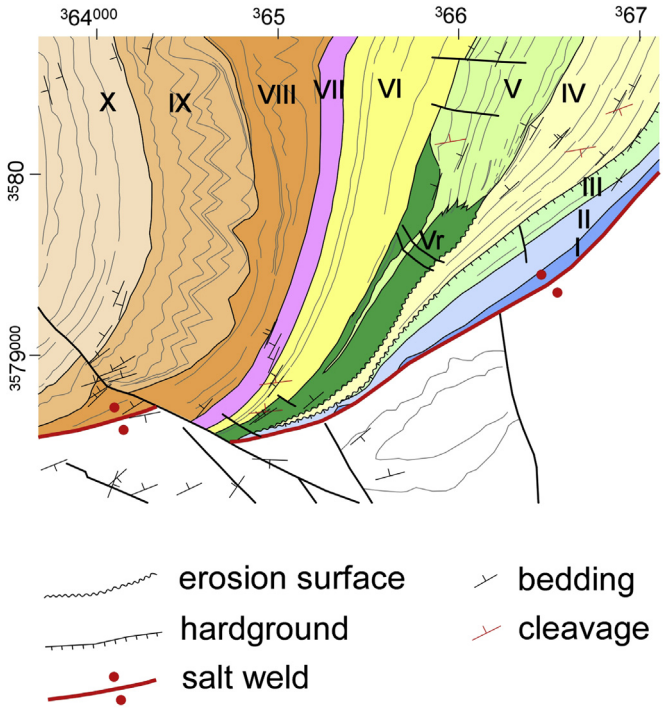

Fig. 15. Detailed map of the southeastern margin of the Azag minibasin showing thinning of stratigraphic units towards the former diapiric margin and the erosional truncations at the base of units IV and V. The bed fanning geometries and the gentle unconformity angles conform to wedge-type halokinetic sequences (in the sense of Giles and Rowan, 2012). UTM coordinates, zone 30.

reefal or calcarenite platforms of units V and VI that grew in the topographic highs passing rapidly into the slope and basinal facies (Fig. 14b and c). Indeed the absence of breccias with Triassic clasts indicates that either the salt walls were often covered by a veneer of shallow-water sediments or that the Triassic Keuper rocks did not form a significant relief if exposed, due to the balancing sedimentation rate and to the weak nature of the Keuper shale and evaporite. At variance to the map presented by Bernasconi (1983), the Azag minibasin does not contain significant layers of conglomerate or breccia —sediment gravity flow deposits are composed of resedimented platform deposits downslope from the aggrading or prograding platform margins—, which is consistent with relatively high sedimentation rates in relation with diapir-rise rates and with the wedge halokinetic geometries observed.

The siliciclastic-dominated unit VII represents a turning point in the basin evolution with a relative reduction of the differential relief between the diapiric salt-ridges and the basin depocenter produced by the evacuation of salt. Progradation of the distal deltaic lobes at this time suggests a relative regression as cited by Stanley (1981) near Rich, which resulted in the shutdown of the carbonate factory and the rapid basin infilling by stacking of deltaic lobes. The siliciclastic material were sourced from the west according to Brechbühler et al. (1988). The basin profile and the submarine relief between the former reef platforms and the basin was levelled, allowing the rapid progradation of the shallow water oolitic bars and patch reefs of unit VIII into the minibasin center, on former basinal areas (Fig. 14c). As the basin deepened, the shallow carbonate factory during deposition of the units IX and X, consisting in oolitic-skeletal bars, was confined again to the diapiric ridges of the basin margins (Figs. 5, 6 and 11), while the depocenter of the basin turned at times into a silled basin with restricted water circulation and oxygen-deficient bottom-sea conditions. These conditions favored the sedimentation of the black mudstones of unit IX and the marls and marly limestones of the unit X.

Detailed correlation of the Bajocian succession of the Azag minibasin with neighboring basins is not yet available, and hence the differential thickness of the Bajocian with respect to the Foum Tillicht and Rich units cannot be evaluated on the lack of key levels for correlation to date. In contrast to the Azag minibasin, in the High Atlas of Rich the Bajocian records a general shallowing (Ait Addi and Chafiki, 2013). This, together with the lower elevation of the preserved Jurassic overburden of the Rich and Foum Tillicht units with respect to Azag, leads to envisage the Azag minibasin as a more rapidly subsiding salt-withdrawal depocenter than the other units (Fig. 14b and c).

Dogger and younger red beds are never preserved in the internal part of the High Atlas near Rich, while they are common more to the west along the rift (e.g. at Imilchil, see location in Fig. 1) or in the northern and southern margins of the High Atlas. This suggests that in this axial part of the rift either the post-Jurassic erosion reached a deeper level or that the downbuilding episode in the minibasins of the Rich High Atlas was maximum in the Bajocian-early Bathonian? interval and terminated before red bed sedimentation proceeded elsewhere in the Atlas rift. The basement structure underlying the Azag minibasin and adjacent salt walls is speculative due to the large uncertainties associated to a plausible strong decoupling between basement and the Jurassic basin structure, and to the superposition of extensional and compressional episodes that has affected the region. As discussed above, basement normal faulting is likely (reference geometries of sub-salt faulting have been illustrated in the Triassic of the Marrakech High Atlas by Domènech et al., 2015), and so is basement-involved orogenic buckle folding, as observed in the Mougueur massif (El Kochri and Chorowicz, 1988; Teixell et al., 2003). Grounding of the bottom of the minibasin is likely as the minibasin depth of 1–1.5 km obtained by cross-section construction is consistent with the depth to basement inferred for the Rich area from wide-angle seismic data (Ayarza et al., 2014). The occurrence of Jurassic gabbro in the Keuper stock south of Jebel Tirrourdine (Bernasconi, 1983) (location in Fig. 16) suggests that at least the northern salt wall bordering the Azag minibasin was originally linked to a deep extensional fault.

There is no record of activity of the Azag basin and flanking diapirs during the late Jurassic and the Cretaceous. During the latest Cretaceous to Cenozoic orogeny the Atlas region was submitted to regional N-S-oriented compression. It is likely that during this stage, orogenic shortening in the Azag area was accommodated primarily by diapir squeezing, leading to salt welding and bed oversteepening of the diapir flanks (Fig. 14d). Any newly extruded salt was probably dissolved near the surface. The interior of Azag basin, which was already tilted to the west, was comparatively little deformed, although the N- to NNE-dipping tectonic cleavage, parallel to the orogenic trend of the High Atlas, attests for a component of internal strain. In general, squeezing of diapirs may have accommodated a significant component of shortening in the internal parts of the High Atlas, where previous works centered on the effects of (mild) thrusting and compressional folding (e.g. Schaer, 1987; Teixell et al., 2003).

8. Conclusions

The Azag minibasin of the Jurassic of Morocco provides a field case for marine carbonate sedimentation in relation to salt tectonics. Facies distribution, layer upturning with wedges of growth strata and localized unconformities indicate deposition contemporaneous with diapiric inflation of a polygonal system of salt walls completely enclosing the minibasin. A ca. 3000 m thick lower Lias to Bajocian-p.p. Bathonian? succession filling the basin recorded the evolution of ten stratigraphic units (I to X), which represent

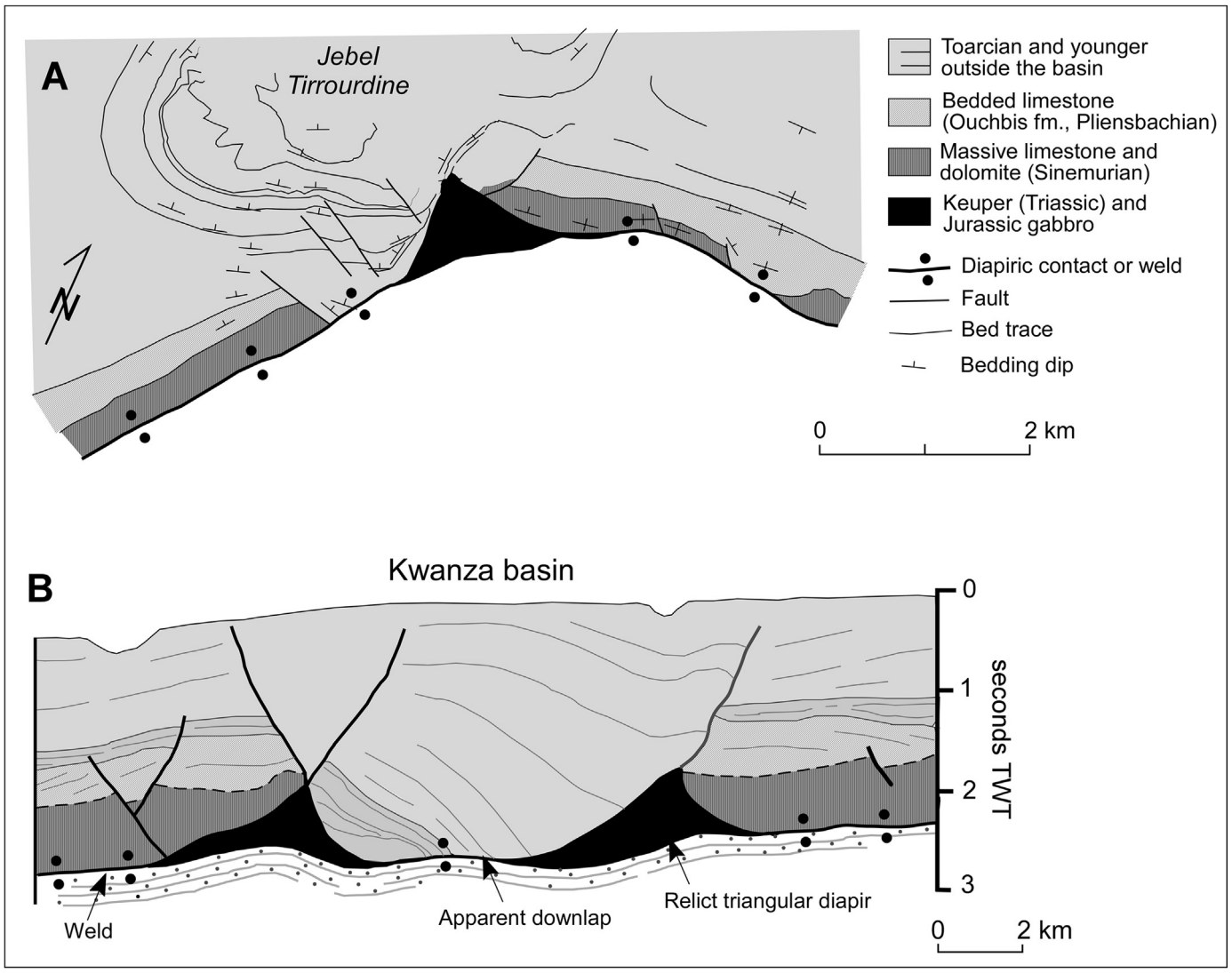

Fig. 16. (A) Detailed map of the boundary between the Azag minibasin and the Foum Tillich unit (location in Fig. 5) showing evidence for diapiric exposure during Jurassic sedimentation. (B) Analogue example of a fallen diapir in Cretaceous-Tertiary sediments of the Kwanza basin, in the continental margin off Angola (redrawn after Duval et al., 1992; Hudec and Jackson, 2011). The missing Lower Jurassic sediments north of the weld in the Foum Tillicht unit (south of Jebel Tirrourdine) suggest that Toarcian and younger sediments lied on top of a passive diapiric high that later subsided, leaving a relict triangular-shaped salt body to the east. The Jebel Tirrourdine structure was later verticalized and welded to the Azag minibasin margin, so the map pattern provides a structural profile.

evolving depositional systems with different paleoenvironments.

The lower units (Units I to III, Hettangian?-Sinemurian to Aalenian) show similar characteristics of equivalent units from areas outside the Azag minibasin (although here much reduced in thickness). A ferruginous hardground of Early Bajocian age and regional extent marks the end of these Lias-earliest Dogger units. The salt-related subsidence peak in the Azag minibasin occurred subsequently, during the Bajocian-early Bathonian?, when up to 2600 m of limestones and marls accumulated at a rate >0.5 mm/a (Units IV to X). Shallow-water reefal limestones developed at the southern and northern basin margins respectively in Units V and VI, grading downslope to fore-reef skeletal calcarenites, resedimented deposits, and marls toward the basin depocenter, attesting for strong bathymetric relief. Unit VII is a unique pro-deltaic terrigenous unit that filled the minibasin and leveled the basin profile. Carbonate sedimentation resumed from unit VIII onwards. Units VIII to X are characterized by the development of shallow-water, cross-bedded oolitic and oolitic-skeletal carbonate bars at the minibasin margins. They grade into outer platform marls and black lime mudstones deposited in semi-enclosed, oxygen-deficient silled conditions toward the basin depocenter.

Facies distribution and evolution in the Azag minibasin obeys to both regional events recorded in the entire high Atlas rift (e.g. Lias drowning events), and local variations in accommodation reflecting diapir inflation and salt-withdrawal/expulsion subsidence (e.g. platform to basin transitions, oolite bar progradation). Halokinetic geometry of units varies from unit to unit and from side to side of the minibasin. In general, sequences are organized in wedge-type sequences, indicative of relative high sedimentation rates. Episodes of enhanced diapiric rise resulted in marked bathymetric relief in the minibasin, with reefal miniplaform developed in the highs, passing rapidly into slope and basinal marls, breccias, debrites and turbidites in the depocentral area. Episodes of subdued inflation resulted in regularization of the basin profile, allowing the progradation of oolitic-skeletal and clastic bars across the basin axis.

Squeezing and welding of the salt walls bounding the Azag minibasin happened after sedimentation, most probably during the

Cenozoic mountain building of the High Atlas. Evidence for strike-slip movements during and after the basin development is lacking. The Azag minibasin is a good field analog for the exploration of carbonate plays in salt-related settings continental margins. Reservoir facies as coral-microbial boundstone, rudstone or well-sorted oolitic grainstone pinch out towards the basin margins and basinwards. Fetid, dark mudstone and shale produced by accelerated subsidence in the upper part of the succession (while in the remainder of the High Atlas a shallowing megasequence was recorded) could have had source rock characteristics and result in a closed system where source and reservoir are contained in the same minibasin.

Acknowledgements

This work was supported by Spanish MINECO grants CGL2010-15416 and CGL2014-54180-P. Cross-sections were constructed with the software *Move*, provided by Midland Valley through the ASI program. Prof. Antonio Goy of the Universidad Complutense de Madrid is thanked for the ammonite classification. Mohamed Charroud and Manuel Julivert are acknowledged for discussion in early visits to the field area. The manuscript benefited from the suggestions by Michael Warsitzka and from the reviews by Klaas Verwer and Gregoire Messager.

References

Ait Addi, A., 1994. Sédimentologie, biostratigraphie et diagenèse carbonatée des faciès du Lias supérieur-Dogger du Haut Atlas d'Errachidia (Maroc). PhD Thesis. University of Tunis II, p. 211.

Ait Addi, A., 2000. Les series du Dogger moyen du Haut Atlas au Nord d'Errachidia (Maroc): lithostratigraphie et sedimentologie d'une nouvelle formation, la formation Tazigzaout. Rev. Géologie Méditerranéenne 27, 57–69.

Ait Addi, A., 2008. Storm deposits: evidence of event sedimentation in the bajocian of the central high Atlas, Morocco. Vol. Jurassica VI 23–32.

Ait Addi, A., Chafiki, D., 2013. Sedimentary evolution and palaeogeography of mid-Jurassic deposits of the Central High Atlas, Morocco. J. Afr. Earth Sci. 84, 54–69.

Ait Addi, A., Chellai, E.H., Ben Ismail, M.H., 1998. Les paléoenvironnements des faciès du Lias supérieur-Dogger du Haut-Atlas d'Errachidia (Maroc). Afr. Geosci. Rev. 5, 39–48.

Ait Brahim, L., Chotin, P., Hinaj, S., Abdelouafi, A., El Adraoui, A., Nakcha, C., Dhont, D., Charroud, M., Sossey Alaoui, F., Amrhar, M., Bouaza, A., Tabyaoui, H., Chaouni, A., 2002. Paleostress evolution in the moroccan african margin from triassic to present. Tectonophysics 357, 187–205.

Andrie, J.R., Giles, K.A., Lawton, T.F., Rowan, M.G., 2012. Halokinetic-sequence Stratigraphy, Fluvial Sedimentology and Structural Geometry of the Eocene, Fluvial Carroza Formation along the La Popa Salt Weld, La Popa Basin, Mexico. Geological Society Special Publication 363, London, pp. 59–80.

Arboleya, M.L., Teixell, A., Charroud, M., Julivert, M., 2004. A structural transect through the high and middle Atlas of Morocco. J. Afr. Earth Sci. 39, 319–327.

Ayarza, P., Alvarez-Lobato, F., Teixell, A., Arboleya, M.L., Tesón, E., Julivert, M., Charroud, M., 2005. Crustal structure under the central High Atlas mountains (Morocco) from geological and gravity data. Tectonophysics 400, 67–84.

Ayarza, P., Carbonell, R., Teixell, A., Palomeras, I., Marti, D., Kchikach, A., Harnafi, M., Levander, A., Gallart, J., Arboleya, M.L., Alcalde, J., Fernández, M., Charroud, M., Amrhar, M., 2014. Crustal thickness and velocity structure across the Moroccan Atlas from long offset wide-angle reflection seismic data: the SIMA experiment. *Geochemistry, Geophysics*. Geosystems 15, 1698–1717.

Babault, J., Teixell, A., Arboleya, M.L., Charroud, M., 2008. A Late Cenozoic age for long-wavelength surface uplift of the Atlas Mountains of Morocco. Terra Nova. 20, 102–107.

Beauchamp, W., Barazangi, M., Demnati, A., El Alji, M., 1996. Intracontinental rifting and inversion: missour basin and Atlas mountains, Morocco. Am. Assoc. Petroleum Geol. Bull. 80, 1459–1482.

Beauchamp, W., Allmendinger, R.W., Barazangi, M., Demnati, A., El Alji, M., Dahmani, M., 1999. Inversion tectonics and the evolution of the High Atlas Mountains, Morocco, based on a geological-geophysical transect. Tectonics 18, 163–184.

Benammi, M., Toto, E., Chakiri, S., 2001. Les chevauchements frontaux du Haut Atlas central marocain: styles structuraux et taux de raccourcissement différentiel entre les versants nord et sud. Comptes Rendus l'Academie Sci. 333 (II), 241–247.

Bernasconi, R., 1983. Géologie du Haut Atlas de Rich (Maroc). PhD Thesis. Univ. de Neuchâtel, p. 107.

Bodin, S., Krencker, F.-N., Kothe, T., Hoffmann, R., Mattioli, E., Heimhofer, U., Kabiri, L., 2016. Perturbation of the carbon cycle during the late Pliensbachian – early Toarcian: new insight from high-resolution carbon isotope records in Morocco. J. Afr. Earth Sci. 116, 89–104.

Bouchouata, A., Canérot, J., Souhel, A., Améras, Y., 1995. Stratigraphie séquentielle et évolution géodynamique du Jurassique dans la région de Talmest-Tazoult (Haut Atlas central, Maroc. Comptes Rendus l'Academie Sci. 320 (II), 749–756.

Brechbühler, Y.A., Bernasconi, R., Schaer, J.P., 1988. Jurassic sediments of the Central High Atlas of Morocco: deposition, burial and erosion history. In: Jacobshagen, V. (Ed.), The Atlas System of Morocco. Springer-Verlag, Berlin, pp. 201–217.

Bromley, R.G., Ekdale, A.A., 1984. Chondrites: a trace fossil indicator of anoxia in sediments. Science 224, 872–874.

Canérot, J., Hudec, M.R., Rockenbauch, K., 2005. Mesozoic diapirism in the Pyrenean orogen: salt tectonics on a transform plate boundary. Am. Assoc. Petroleum Geol. Bull. 89, 211–229.

Christ, N., Immenhauser, A., Amour, F., Mutti, M., Tomás, S., Agar, S.M., Alway, R., Kabiri, L., 2012. Characterization and interpretation of discontinuity surfaces in a Jurassic ramp setting (High Atlas, Morocco). Sedimentology 59, 249–290.

Choubert, G., Faure-Muret, A., 1962. Evolution du domaine atlasique marocain depuis les temps paléozoïques. In: Soc. géol France. Livre a la Mémoire du Professeur Paul Fallot, Memoire hors série, 1, Paris, pp. 447–527.

Crevello, P.D., Harris, P.M., 1984. Depositional models for Jurassic reefal buildups. Third Annual Research Conference Proceedings. In: Ventress, W.P.S., Bebout, D.G., Perkins, C.H. (Eds.), The Jurassic of the Gulf Rim. Gulf Coast Section, SEPM Foundation, pp. 57–102.

Della Porta, G., Merino-Tomé, O., Kenter, J.A.M., Verwer, K., 2013. Lower jurassic microbial and skeletal carbonate factories and platform geometry (Djebel Bou dahar, high Atlas, Morocco). In: Verwer, K., Playton, T.E., Harris, P.M. (Eds.), Deposits, Architecture and Controls of Carbonate Margin, Slope and Basinal Settings. SEPM Special Publication 105, pp. 237–263.

Di Stefano, P., Mindszenty, A., 2000. Fe–Mn-encrusted "Kamenitza" and associated features in the Jurassic of Monte Kumeta (Sicily): subaerial and/or submarine dissolution? Sediment. Geol. 132, 37–68.

Domènech, M., Teixell, A., Babault, J., Arboleya, M.L., 2015. The inverted Triassic rift of the Marrakech High Atlas: a reappraisal of basin geometries and faulting histories. Tectonophysics 663, 177–191.

Dongjie, T., Xiaoying, S., Ganqing, J., Yunpeng, P., Wenhao, Z., 2013. Environment controls on Mesoproterozoic thrombolite morphogenesis: a case study from the North China Platform. J. Palaeogeogr. 2 (3), 275–296.

Dromart, G., 1992. Jurassic deep-water microbial biostromes as flooding markers in carbonate sequence stratigraphy. Palaeogeography, Palaeoclimatology. Palaeoecology 91, 219–228.

Du Dresnay, R., 1964. Les discontinuités de sédimentation pendant le Jurassique, dans la partie orientale du domaine atlasique marocain, leurs conséquences stratigraphiques et leurs relations avec l'orogenèse atlasique. In: Colloque Jurassique, Luxemburg 1962. Publ. Inst. Grand-Ducat, pp. 899–912.

Du Dresnay, R., 1971. Relations paléogéographiques entre sillons atlasiques (Haut et Moyen Atlas) et plate-forme des Hauts Plateaux (Maroc oriental) pendant l'Aalénien et le Bajocien. In: 2ème Colloque Jurassique, France 1967. Mémoires du Bureau des Recherches Géologiques et Minieères. Orléans 75, 147–161.

Duval, B., Cramez, C., Jackson, M.P.A., 1992. Raft tectonics in the Kwanza basin, Angola. Mar. Petroleum Geol. 9, 389–404.

El Kochri, A., Chorowicz, J., 1988. Tectonique synsédimentaire et style éjectif dans la couverture mésozoïque du Haut Atlas oriental (Maroc): exemple de la boutonnière de Mougueur. France 8, t. IV Bull. Soc. Géol. 4, 541–550.

El Kochri, A., Chorowicz, J., 1996. Oblique extension in the Jurassic "trough" of the central and eastern High Atlas (Morocco). Can. J. Earth Sci. 33, 84–92.

Ettaki, M., Chellaï, E.H., Milhi, A., Sadki, D., Boudchich, L., 2000. Le passage Lias moyen–Lias supérieur dans la région de Todrha-Dadès : événements bio-sédimentaires et géodynamiques (Haut Atlas central, Maroc). C. R. Acad. Sci. Paris, Sci. de Terre des planètes 331, 667–674.

Ettaki, M., Ibouh, H., Chellaï, E.H., Milhi, A., 2007. Les structures "diapiriques" liasiques du Haut-Atlas central, Maroc: exemple de la ride d'Ikerzi. Afr. Geosci. Rev. 14, 79–93.

Evans, I., Kendall, C.G.S.T.C., Warme, J.E., 1974. Jurassic sedimentation in the high Atlas mountains of Morocco during early rifting of Africa and north America. Geology 2, 295–296.

Flügel, E., 2004. Microfacies of Carbonate Rocks. Analysis, Interpretation and Application. Springer, Berlin.

Friedman, G.M., Shulka, V., 1980. Significance of authigenic quartz euhedra after sulphates: example from the Lockport Formation (Middle Silurian) of New York. J. Sediment. Petrology 50, 1299–1304.

Frizon de Lamotte, D., Saint Bezar, B., Bracène, E., Mercier, E, E., 2000. The two main steps of the Atlas building and geodynamics of the western Mediterranean. Tectonics 19, 740–761.

Frizon de Lamotte, D., Leturmy, P., Missenard, Y., Khomsi, S., Ruiz, G., Saddiqi, O., Guillocheau, F., Michard, A., 2009. Mesozoic and Cenozoic vertical movements in the Atlas system (Algeria, Morocco, Tunisia): an overview. Tectonophysics 475, 9–28.

Ge, H., Jackson, M.P.A., Vendeville, B.C., 1997. Kinematics and dynamics of salt tectonics driven by progradation. Am. Assoc. Petroleum Geol. Bull. 81, 398–423.

Giles, K.A., Lawton, T.F., 2002. Halokinetic sequence stratigraphy adjacent to El Papalote Diapir, northeastern Mexico. Am. Assoc. Petroleum Geol. Bull. 86, 823–840.

Giles, K.A., Rowan, M.G., 2012. Concepts in Halokinetic-sequence Deformation and Stratigraphy. Geological Society Special Publication 363, London, pp. 7–32.

Gómez-Cabrera, P.T., Jackson, M.P.A., 2008. Regional Neogene salt tectonics in the offshore Salina del Istmo Basin, southeastern Mexico. In: Bartolini, C., Román Ramos, J.R. (Eds.), Petroleum Systems in the Southern Gulf of Mexico. American Association of Petroleum Geologists Memoi 90, pp. 1–28.
Haddoumi, H., Charrière, A., Mojon, P.-O., 2010. Stratigraphie et sédimentologie des «Couches rouges» continentales du Jurassique-Crétacé du Haut Atlas central (Maroc): implications paléogéographiques et géodynamiques. Geobios 43, 433–451.
Hailwood, E.A., Mitchell, J.G., 1971. Paleomagnetic and radiometric dating results from Jurassic intrusions in south Morocco. Geophys. J. R. Astron. Soc. 24, 351–364.
Hudec, M.R., Jackson, M.P.A., 2007. Terra infirma: understanding salt tectonics. Earth-Science Rev. 82, 1–28.
Hudec, M.R., Jackson, M.P.A., 2011. The salt mine: a digital Atlas of salt tectonics. The University of Texas at Austin, Bureau of Economic Geology, Udden Book Series No. 5-American Association of Petroleum Geologists Memoir 99, Austin.
Hudec, M.R., Jackson, M.P.A., Schultz-Ela, D.D., 2009. The paradox of minibasin subsidence into salt: clues to the evolution of crustal basins. Geol. Soc. Am. Bull. 121, 201–221.
Ibouh, H., Laville, E., Amrhar, M., Bouabdelli, M., 2008. Migration des aires de sédimentation au cours du Dogger dans le Haut Atlas central (Maroc): exemples du synclinal d'Azag n'Oufoulloussene et de Michlifène. Notes Mém. Serv. Géol. Maroc 527, 73–82.
Igmoullan, B., Sadki, D., Fedan, B., Chellai, E.H., 2001. Evolution géodynamique du Haut-Atlas de Midelt (Maroc) pendant le Jurassique: un exemple d'interaction entre la tectonique et l'eutatisme. Bull. Inst. Sci. Rabat, Sect. Sci. Terre 23, 47–54.
Jakubowicz, M., Belka, Z., Berkowski, B., 2014. *Frutexites* encrustations on rugose corals (Middle Devonian, southern Morocco): complex growth of microbial microstromatolites. Facies 60, 631–650.
Jenny, J., Le Marrec, A., Monbaron, M., 1981. Les Couches rouges du Jurassique moyen du Haut Atlas central (Maroc): corrélations lithostratigraphiques, éléments de datations et cadre tectono-sédimentaire. France 7, t. XXIII Bull. Soc. géol 6, 627–639.
Kernen, R.A., Giles, K.A., Rowan, M.G., Lawton, T.W., Hearon, T.E., 2012. Depositional and Halokinetic-sequence Stratigraphy of the Neoproterozoic Wonoka Formation Adjacent to Patawarta Allochthonous Salt Sheet, Central Flinders Ranges, South Australia. Geological Society Special Publication 363, London, pp. 81–105.
Lachkar, N., Guiraud, M., El Harfi, A., Dommergues, J.-L., Dera, G., Durlet, C., 2009. Early Jurassic normal faulting in a carbonate extensional basin: characterization of tectonically driven platform drowning (High Atlas rift, Morocco). J. Geol. Soc. 166, 413–430.
Laville, E., 1985. Evolution sédimentaire, tectonique et magmatique du bassin jurassique du Haut Atlas, Maroc: modèle en relais multiples de décrochements. Thèse Doct.. Univ. de Montpellier II, p. 166.
Laville, E., Piqué, A., 1992. Jurassic penetrative deformation and Cenozoic uplift in the Central High Atlas (Morocco): a tectonic model. Structural and Orogenic inversions. Geol. Rundsch. 81, 157–170.
Laville, E., Piqué, A., Amrhar, M., Charroud, M., 2004. A restatement of the Mesozoic Atlas rifting (Morocco). J. Afr. Earth Sci. 38, 145–153.
Mattauer, M., Tapponier, P., Proust, F., 1977. Sur les mécanismes de formation des chaines intracontinentales. L'exemple des chaines atlasiques du Maroc. France 7, t. 19 Bull. Soc. Géol. 3, 521–526.
Matthews, W.J., Hampson, G.J., Trudgill, B.D., Underhill, J.R., 2007. Controls on fluviolacustrine reservoir distribution and architecture in passive salt-diapir provinces: insights from outcrop analogs. Am. Assoc. Petroleum Geol. Bull. 91, 1367–1403.
Mehdi, M., Neuweiler, F., Wilmsen, M., 2003. Les formations du Lias inférieur du Haut Atlas central de Rich (Maroc): précisions lithostratigraphiques et étapes de l'évolution du basin. France t. 174 Bull. Soc. Géol. 3, 227–242.
Merino-Tomé, O., Della Porta, G., Kenter, J.A.M., Verwer, K., Harris, P.M., Adams, E.W., Playton, T., Corrochano, D., 2012. Sequence development in an isolated carbonate platform (Lower Jurassic, Djebel Bou Dahar, High Atlas, Morocco): influence of tectonics, eustacy and carbonate production. Sedimentology 59, 118–155.
Michard, A., Ibouh, H., Charrière, A., 2011. Syncline-topped anticlinal ridges from the high Atlas: a moroccan conundrum, and inspiring structures from the syrian arc, Israel. Terra Nova. 23, 314–323.
Milhi, A., Ettaki, M., Chellaï, E.H., Hadri, M., 2002. Les formations lithostratigraphiques jurassiques du Haut-Atlas central (Maroc): corrélations et reconstructions paléogéographiques. Rev. Paléobiologie 21, 241–256.
Moragas, M., Vergés, J., Saura, E., Martín-Martín, J.-D., Messager, G., Merino-Tomé, O., Suárez-Ruiz, I., Razin, Ph, Grélaud, C., Malaval, M., Jousssiaume, R., Hunt, D.W., 2016. Jurassic rifting to post-rift subsidence analysis in the Central High Atlas and its relation to salt diapirism. Basin Res. http://dx.doi.org/10.1111/bre.12223.
Najarro, M., Rosales, I., Martín-Chivelet, J.M., 2011. Major palaeoenvironmental perturbation in an early Aptian carbonate platform: prelude of the Oceanic Anoxic Event 1a? Sediment. Geol. 235, 50–71.
Neuweiler, F., Mehdi, M., Wilmsen, M., 2001. Facies of liassic sponge mounds, central high Atlas, Morocco. Facies 44, 243–264.
Olivier, N., Hantzpergue, P., Gaillard, Ch, Pittet, B., Leinfelder, R.R., Schmid, D.U., Werner, W., 2003. Microbialite morphology, structure and growth: a model of the upper jurassic reefs of the chay peninsula (western France). Palaeogeography, palaeoclimatology, Palaeoecology 193, 383–404.
Olivier, N., Martin-Garin, B., Colombié, C., Cornée, J.-J., Giraud, F., Schnyder, J., Kabbachi, B., Ezaidi, K., 2013. Ecological succession evidence in an Upper Jurassic coral reef system (Izwarn section, High Atlas, Morocco). Geobios 45, 555–572.
Piqué, A., Charroud, M., Laville, E., Aït Brahim, L., Amrhar, M., 2000. The Tethys southern margin in Morocco; Mesozoic and Cainozoic evolution of the Atlas domain. In: Crasquin-Soleau, S., Barrier, E. (Eds.), Peri-tethys Memoir 5: New Data on Peri-tethyan Sedimentary Basins. Mém. Mus. natn. Hist. Nat. 182, Paris, pp. 93–106.
Pleş, G., Mircescu, C.V., Bucur, I.I., Săsăran, E., 2013. Encrusting micro-organisms and microbial structures in upper jurassic limestones from the southern carpathian (Romania). Facies 59, 19–48.
Poprawski, Y., Cristophe, B., Jaillard, E., Matthieu, G., Lopez, M., 2016. Halokinetic sequences in carbonate systems: an example from the middle albian bakio breccias formation (basque country, Spain). Sediment. Geol. 334, 34–52.
Préat, A., Mamet, B., De Ridder, C., Boulvain, F., Gillan, D., 2000. Iron bacterial and fungal mats, Bajocian stratotype (Mid-Jurassic, northern Normandy, France). Sediment. Geol. 137, 107–126.
Quiquerez, A., Sarih, S., Allemand, P., García, J.-P., 2013. Fault rate controls on carbonate gravity-flow deposits of the Liassic of Central High Atlas (Morocco). Mar. Petroleum Geol. 43, 349–369.
Reitner, J., 1988. A comparative study of the diagenesis in diapir-influenced reef atolls and fault block reef platform in the Late Albian of the Vasco-Cantabrian basin (northern Spain). In: Schroeder, J.H., Purser, B.H. (Eds.), Reef Diagenesis. Springer-Verlag, Berlin, pp. 186–209.
Reolid, M., Abad, I., Martín-García, J.M., 2008. Palaeoenvironmental implications of ferruginous deposits related to a middle-late jurassic discontinuity (prebetic zone, betic cordillera, southern Spain). Sediment. Geol. 203, 1–16.
Ribes, Ch, Kergaravat, Ch, Bonnel, C., Crumeyrolle, Ph, Callot, J.-P., Poisson, A., Temiz, H., Ringenbach, J.-C., 2015. Fluvial sedimentation in a salt-controlled mini-basin: stratal patterns and facies assemblages, Sivas Basin, Turkey. Sedimentology 62, 1513–1545.
Riding, R., 2000. Microbial carbonates: the geological record of calcified bacterial-algal mats and biofilms. Sedimentology 47, 179–214.
Ringenbach, J.-C., Salel, J.F., Kergaravat, C., Ribes, C., Bonnel, C., Callot, J.-P., 2013. Salt tectonics in the Sivas Basin, Turkey; outstanding seismic analogues from outcrops. First Break 31, 57–65.
Rosales, I., Mehl, D., Fernández-Mendiola, P.A., García-Mondéjar, J., 1995. An unusual poriferan community in the Albian of Islares (north Spain): palaeoenvironmental and tectonic implications. *Palaeogeography, Palaeoclimatology*. Palaeoecology 119, 47–61.
Rowan, M.G., Vendeville, B.C., 2006. Foldbelts with early salt withdrawal and diapirism: physical model and examples from the northern Gulf of Mexico and the Flinders Ranges, Australia. Mar. Petroleum Geol. 23 (9–10), 871–891.
Rowan, M.G., Giles, K.A., Hearon, I.V.,T.E., Fiduk, J.C., 2016. Megaflaps adjacent to salt diapirs. Am. Assoc. Petroleum Geol. Bull. 100, 1723–1747.
Sadki, D., 1992. Les variations de faciès et les discontinuités de sédimentation dans le Lias – Dogger du Haut-Atlas central (Maroc) : chronologie, caractérisation, corrélations. France t. 163 Bull. Soc. géol 2, 179–186.
Sadki, D., 1996. Le Haut-Atlas central (Maroc). Stratigraphie et paleontologie du Lias Supérieur et du Dogger Inférieur. *Dynamique du bassin et des peuplements*. Docum. Lab. Géol, Lyon 142, p. 245.
Saura, E., Vergés, J., Martin-Martin, J.D., Messager, G., Moragas, M., Razin, P., Grelaud, C., Joussiaume, R., Malaval, M., Homke, S., Hunt, D.W., 2014. Syn- to post-rift diapirism and minibasins of the Central High Atlas (Morocco): the changing face of a mountain belt. J. Geol. Soc. 171, 97–105.
Saura, E., Ardèvol i Oro, Ll, Teixell, A., Vergés, J., 2016. Rising and falling diapirs, shifting depocenters, and flap overturning in the Cretaceous Sopeira and Sant Gervàs subbasins (Ribagorça Basin, southern Pyrenees). Tectonics 35, 638–662.
Schaer, J.P., 1987. Evolution and structure of the high Atlas of Morocco. In: Schaer, J.P., Rodgers, J. (Eds.), The Anatomy of Mountain Ranges. Princeton Univ. Press, pp. 107–127.
Stanley, R.G., 1981. Middle jurassic shoaling of the central high Atlas sea near rich, Morocco. J. Sediment. Petrology 51, 895–907.
Studer, M.A., 1987. Tectonique et Pétrographie des roches sédimentaires, éruptives et métamorphiques de la region de Tounfite-Tirrhist (Haut Atlas central mésozoïque, Maroc). Notes Serv. Géol. Maroc. 43 (321), 65–197.
Tari, G., Molnar, J., Ashton, P., 2003. Examples of Salt Tectonics from West Africa: a Comparative Approach. Geological Society Special Publication 207, London, pp. 85–104.
Tari, G., Jabour, H., 2013. Salt Tectonics in the Atlantic Margin of Morocco. Geological Society Special Publication 369, London, pp. 337–353.
Teixell, A., Arboleya, M.L., Julivert, M., Charroud, M., 2003. Tectonic shortening and topography in the central High Atlas (Morocco). Tectonics 22 (5), 1051, 1010.1029/2002TC001460.
Teixell, A., Ayarza, P., Zeyen, H.,M., Fernandez, M., Arboleya, M.L., 2005. Effects of mantle upwelling in a compressional setting: the Atlas Mountains of Morocco. Terra Nova 17, 456–461.
Tesón, E., Teixell, A., 2008. Sequence of thrusting and syntectonic sedimentation in the eastern Sub-Atlas thrust belt (Dades and Mgoun valleys, Morocco). Int. J. Earth Sci. 97, 103–113.
Tomás, S., Homann, M., Mutti, M., Amour, F., Christ, N., Immenhauser, A., Agar, S.M., Kabiri, L., 2013. Alternation of microbial mounds and ooid shoals (Middle Jurassic, Morocco): response to paleoenvironmental changes. Sediment. Geol. 294, 68–82.
Trudgill, B.D., 2011. Evolution of salt structures in the northern Paradox Basin:

controls on evaporite deposition, salt wall growth and supra-salt stratigraphic architecture. Basin Res. 23, 209–238.
Verwer, K., Merino-Tomé, O., Kenter, J.A.M., Della Porta, G., 2009. Evolution of a high-relief carbonate platform slope using 3D digital outcrop models: lower Jurassic Djebel Bou Dahar, High Atlas, Morocco. J. Sediment. Res. 79, 416–439.
Warme, J.E., 1988. Jurassic carbonate facies of the central and eastern high Atlas rift, Morocco. In: Jacobshagen, V. (Ed.), The Atlas System of Morocco. Springer-Verlag, Berlin, pp. 169–199.
Warsitzka, M., Kley, J., Kukowski, N., 2013. Salt diapirism driven by differential loading- Some insights from analogue modelling. Tectonophysics 591, 83–97.
Warsitzka, M., Kley, J., Kukowski, N., 2015. Analogue experiments of salt flow and pillow growth due to basement faulting and differential loading. Solid earth.. 6, 9–31.
Wignall, P.B., Newton, R., Brookfield, M.E., 2005. Pyrite framboid evidence for oxygen-poor deposition during the Permian-Triassic crisis in Kashmir. Palaeogeography, Palaeoclimatology, Palaeoecology 216, 183–188.
Wilkin, R.T., Barnes, H.L., 1997. Formation processes of framboidal pyrite. Geochem. Cosmochimica Acta 61, 323–339.
Wilmsen, M., Blau, J., Meister, C., Mehdi, M., Neuweiler, F., 2002. Early jurassic (sinemurian to toarcian) ammonites from the central high Atlas (Morocco) between Er-Rachidia and rich. Rev. Paléobiologie 21, 149–175.
Wilmsen, M., Neuweiler, F., 2008. Biosedimentology of the Early Jurassic post-extinction carbonate depositional system, central High Atlas rift basin, Morocco. Sedimentology 55, 773–807.